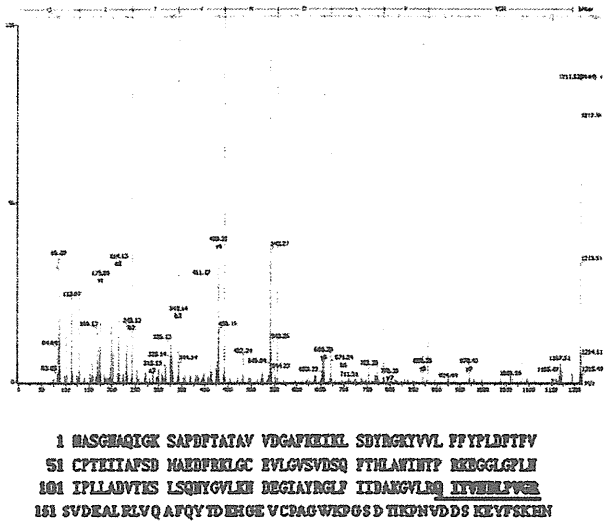

Figure 3. Mass spectrometry of the stathmin-1 spot. MS/MS signals were derived from the parent ion, for which the amino acid sequence, QIT-VNDLPVGR, was deduced based upon these ions in tandem MS spectrum. MS/MS spectrum of stathmin-1 is shown. Peptide was identified by matrix-assisted laser desorption/ionization time of flight/time of flight MS/MS and matched with residues 140-150 of stathmin-1. Protein sequence of stathmin-1 is shown, and matched MS/MS fragmentation is underlined. The peptide mass fingerprinting and the MS/MS maps of stathmin-1 were combined to confirm the MS results.

Disparate Abundance of Stathmin-1$^+$DBA-Lectin$^+$ Cells between CBA/J×BALB/c and CBA/J×DBA/2J Matings

As shown in Figure 5, the presence of stathmin-1$^+$DBA-lectin$^+$ cells was confirmed in CBA/J×BALB/c and CBA/J×DBA/2J matings using multivision IHC. The DBA-lectin$^+$ cells were stained green, stathmin-1$^+$ cells were stained red, and double-positive cells were yellow in the merged images. Nuclei were stained blue by 4′,6-diamidino-2-phenylindole.

However, the frequency of stathmin-1$^+$DBA-lectin$^+$ cells was significantly higher in CBA/J×BALB/c matings, whereas DBA-lectin$^+$stathmin-1$^+$ cells were rare in CBA/J×DBA/2J matings. As indicated in Figure 5, A-D, DBA-lectin$^+$ cells (green) are more dominant than stathmin-1$^+$ cells in both mating combinations. However, red (stathmin-1) is robust in CBA/J×BALB/c matings but either absent or faint in CBA/J×DBA/2J matings. In the merged images, the relative number of stathmin-1$^+$DBA-lectin$^+$ cells (yellow) is higher in CBA/J×BALB/c matings (Figure 5, A and B) than in CBA/J×DBA/2J matings (Figure 5, C and D).

The murine cells positive for DBA-lectin were scattered intensively in decidual basalis tissue and in the mesometrial lymphoid aggregate of pregnancy in both matings, whereas no DBA-lectin$^+$ cells were observed in placenta tissue (region P) (Figure 5, E and F).[22]

The mean density of stathmin-1$^+$DBA-lectin$^+$ cells was determined using Image-Pro Plus 6.0 (Media Cybernetics Inc., Bethesda, MD). The mean ± SD density of the double-positive cells was significantly higher in CBA/J×BALB/c matings than in CBA/J×DBA/2J matings (9.6 ± 5.5 versus 1.0 ± 0.9; $P < 0.01$) (Figure 5G).

The Distribution Pattern of Stathmin-1$^+$ Cells in the Human CD56$^+$ Cell Population

The distribution pattern of stathmin-1$^-$CD56$^+$ and stathmin-1$^+$CD56$^+$ cells was evaluated by means of double-vision IHC. Stathmin-1$^+$CD56$^+$ cells were observed in human decidua from RSA patients (Figure 6, A–D) and those with normal early pregnancy (Figure 6, E–H) but were more frequently detected in the latter. Stathmin-1$^-$CD56$^+$ and stathmin-1$^+$CD56$^+$ cells were mainly detected in tissues near blood vessels, whereas stathmin-1$^+$CD56$^+$ cells were seldom found in tissues where there were almost no blood vessels. The mean density of stathmin-1$^+$CD56$^+$ cells was determined using Image-Pro Plus 6.0. The mean ± SD density of the double-positive cells was significantly higher in normal early pregnancy than in RSA patients (13.6 ± 7.2 versus 1.0 ± 0.7; $P < 0.01$) (Figure 6I).

Effects of Anti–Stathmin-1 Antibody Treatment on Embryo Loss

The mean ± SD percentage of embryo resorption was higher in CBA/J×DBA/2J matings when stathmin-1 protein was inhibited using a neutralizing antibody (with inhibition: 42.1% ± 21.2%, 32 of 76; control: 21.8% ± 12.4%, 17 of 78; $P < 0.05$) (Figure 7). The change in the percentage of embryos lost in the CBA/J×BALB/c and CBA/J×CBA/J matings treated with the stathmin-1 neutralizing antibody did not reach statistical significance (CBA/J×BALB/c, with inhibition: 14.1% ± 10.1%, 11 of 78; CBA/J×BALB/c, control: 8.5% ± 5.4%, 6 of 71; CBA/J×CBA/J, with inhibition: 9.9% ± 6.5%, 8 of 75; CBA/J×CBA/J, control: 7.3% ± 6.5%; 6 of 79) (Figure 7).

Discussion

Stathmin is reportedly expressed in the glandular epithelium and stromal cells of human endometrial tissue by cytotrophoblasts and extravillous trophoblasts but not by syncytiotrophoblasts.[6] When stromal cells isolated from normal endometrial tissues were previously cultured and stimulated to decidualize by progesterone plus estrogen or cAMP their total and phosphorylated stathmin levels decreased

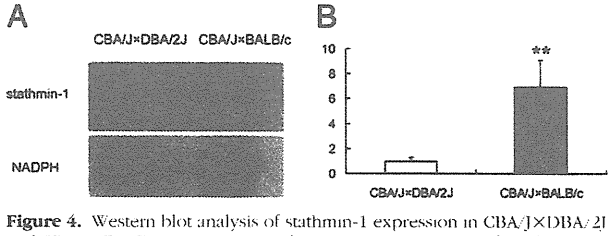

Figure 4. Western blot analysis of stathmin-1 expression in CBA/J×DBA/2J and CBA/J×BALB/c matings. **A:** Stathmin-1 expression is significantly down-regulated in CBA/J×DBA/2J mice compared with CBA/J×BALB/c mice. NADPH was used as an internal loading control. **B:** Histogram showing the relative expression level of stathmin-1 protein in CBA/J×BALB/c and CBA/J×DBA/2J mice as determined using Image-Pro Plus 6.0. The stathmin-1 protein level is a mean ± SD 6.9 ± 2.2–fold higher in CBA/J×BALB/c mice than in CBA/J×DBA/2J mice as determined using densitometric analysis (**$P < 0.01$). Experiments were independently repeated four times for each group. Error bars represent SD.

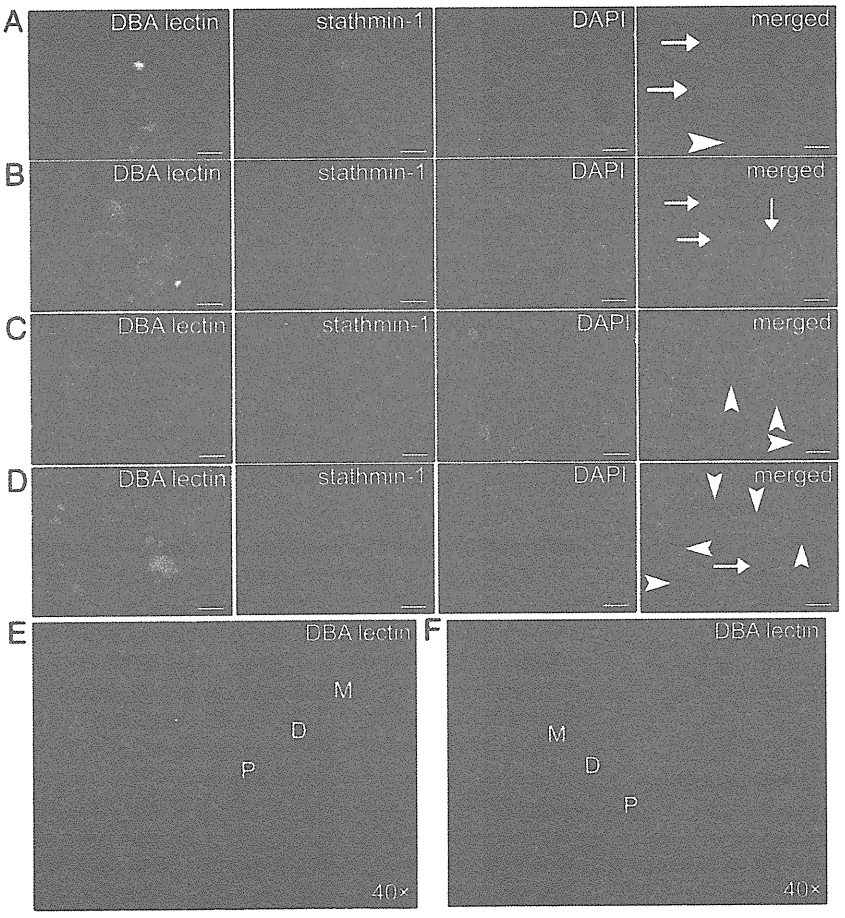

Figure 5. The distribution pattern of stathmin-1$^+$DBA-lectin$^-$ cells in murine tissue. In multivision IHC, uNK cells were stained green with FITC-conjugated DBA-lectin, stathmin-1$^-$ cells were indirectly stained red with rabbit anti-stathmin-1 and PE-conjugated antirabbit IgG, and nuclei were stained blue with DAPI. In the merged images, stathmin-1$^-$DBA-lectin$^+$ cells appear yellow or orange (**arrows**) and stathmin-1$^+$DBA-lectin$^-$ cells are green (**arrowheads**). **A** and **B:** From CBA/J×BALB/c mice. **C** and **D:** From CBA/J×DBA/2J mice. **A** and **B** as well as **C** and **D** are presented to show reproducibility. Scale bar = 10 μm. The DBA-lectin$^+$ cells were dominant in both mating combinations compared with stathmin-1$^+$ cells and other indicated cell subsets. In the merged images from CBA/J×DBA/2J matings, red (stathmin-1$^+$) is either absent or faint. In contrast, red (stathmin-1$^+$) is robust in the images from CBA/J×BALB/c matings and readily yield yellow and is visible in the presence of green (DBA-lectin$^+$). **E:** From CBA/J×BALB/c mice. **F:** From CBA/J×DBA/2J mice. Original magnification, ×40 (**E** and **F**). P, placenta; D, decidual basalis; M, mesometrial lymphoid aggregate of pregnancy. The DBA-lectin$^+$ cells were scattered intensively in regions D and M in both matings but no positive cells were found in region P. **G:** The mean density of stathmin-1$^+$DBA-lectin$^-$ cells as determined using Image-Pro Plus 6.0. Error bars represent SD. $^{**}P < 0.01$.

Stathmin silencing in primary stromal cells using small interfering RNA before the cells are exposed to decidualizing agents also markedly suppresses decidualization, suggesting that stathmin may play a key role in decidualization.[6] Stathmin overexpression favors microtubule destabilization, whereas decreased stathmin expression favors elongated, bundled microtubules and an increased ratio of polymerized to soluble tubulin.[23] Immunohistochemical analyses using a rat model previously revealed that stathmin-1 is exclusively localized in decidual cells, especially in the primary decidual zone surrounding the embryo with markedly more intense staining on day E9.5 than on day E7.5. On day E14.5, when the endometrial stromal cells have completely differentiated into decidual cells, the staining of decidual cells is faint.[7] An experiment in the delayed implantation pregnant rat model revealed low uterine stathmin expression that was increased after implantation, which was induced by 17β-estradiol administration to progesterone-primed animals. Furthermore, decidualization in the pseudopregnant rat, induced by intrauterine oil infusion, stimulates stathmin expression. Stathmin expression clearly increases in the uterus when stimulated by embryo implantation and decidualization and is believed to play a role in the early stages of pregnancy.[8]

Herein, we demonstrated by using two-color flow cytometry that stathmin-1 is expressed intensively in uNK cells isolated from mouse models. The uNK cells were previously purified by means of MACS and were confirmed to be CD3$^-$CD49b$^+$ cells.[11] In multivision IHC using decidual samples from humans and CD56 as a pan marker for human NK cells, the distribution pattern of stathmin-1$^+$CD56$^+$ cells was consistent with the reported roles of NK cells in the pregnant uterus. Under physiologic conditions, NK cells are the dominant cell population up to mid-gestation in the pregnant uterus and are believed to participate in blood vessel remodeling.[24–26] The origin of these NK cells is unclear. A previous study demonstrated that NK cells from extrauterine tissue migrate into the pregnant uterus.[26] Thus, we conclude that a fraction of the stathmin-1$^+$ cells are actually uNK cells, which immigrate into the pregnant uterus at the early stages of pregnancy and are involved in the modulation of implantation and decidualization.

The percentage of stathmin-1$^+$ cells in the uNK cell population was significantly higher in CBA/J×BALB/c matings than in abortion-prone CBA/J×DBA/2J matings. In addition, the intensity of stathmin-1 expression was stronger in CBA/J×BALB/c matings than in CBA/J×DBA/2J matings, as indicated by 2-DE and Western blot analysis. This differential stathmin-1 expression correlated with the difference in the embryo loss rate, which was lower in CBA/J×BALB/c matings than in CBA/J×DBA/2J matings. Thus, the reduced stathmin-1 production in uNK cells correlates with the increased failure of healthy embryos by CBA/J×DBA/2J matings. Furthermore, stathmin-1 inhibition with a neutralizing

antibody increased the percentage of embryo loss in CBA/J×DBA/2J matings, but no such trend was observed in CBA/J×BALB/c, CBA/J×CBA/J, or syngeneic CBA/J×CBA/J matings. These results suggest that stathmin-1 may be a key regulator in the maintenance of allogeneic pregnancy tolerance, at least in CBA/J×DBA/2J matings. In CBA/J×BALB/c matings, the increase in embryo resorption after stathmin-1 inhibition did not reach statistical significance. Although the reason for this is unclear, it may be explained by the difference in the uNK cell functional status between CBA/J×DBA/2J and CBA/J×BALB/c matings, indicating the presence of a fragile system of stathmin-1–mediated modulation in CBA/J×DBA/2J matings.

In multivision IHC, colocalization of stathmin-1 and DBA-lectin was confirmed in murine decidual tissue from both mating combinations. However, the frequency of

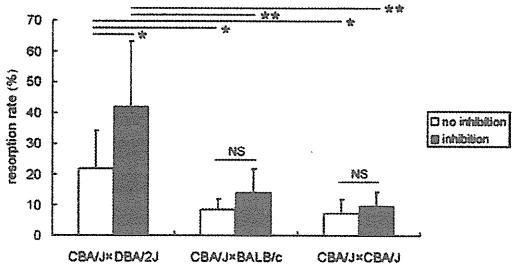

Figure 7. Effect of anti–stathmin-1 antibody treatment on the embryo resorption rate. No inhibition, multiple injections with isotype control antibody; inhibition, multiple injections with neutralizing antibody. In the no-inhibition CBA/J×DBA/2J group, the percentage of embryo loss was significantly higher than that in the no-inhibition CBA/J×BALB/c and CBA/J×CBA/J groups, confirming that CBA/J×DBA/2J mice are prone to abortion. The percentage of embryo loss was increased after stathmin-1 inhibition in CBA/J×DBA/2J mice ($^{*}P < 0.05$, $^{**}P < 0.01$), but the trend of embryo loss increase did not reach statistical significance in CBA/J×BALB/c or CBA/J×CBA/J mice. $n = 8$ per group. Error bars represent SD.

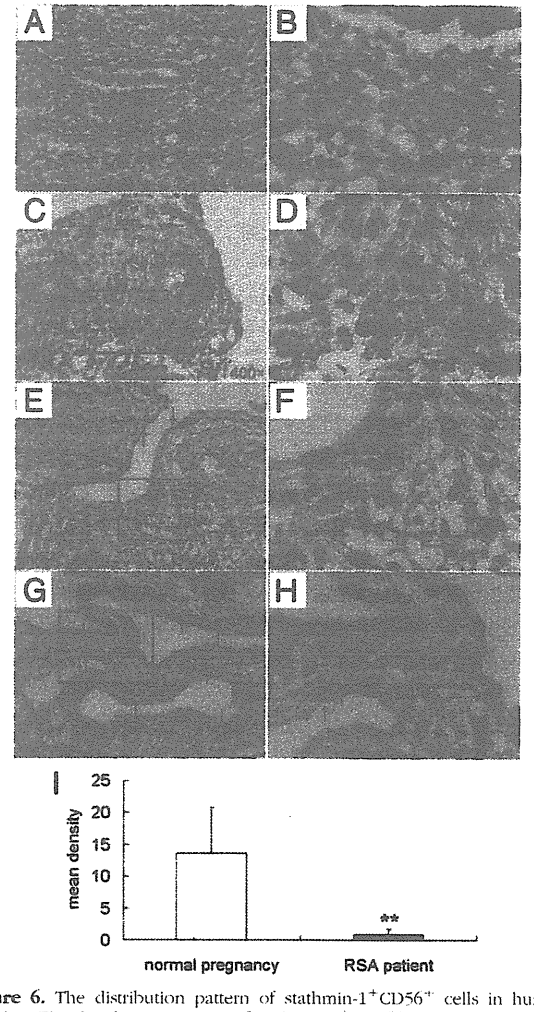

Figure 6. The distribution pattern of stathmin-1^{+}CD56^{+} cells in human decidua. The distribution pattern of stathmin-1^{+}CD56^{+} cells was examined by means of double-staining IHC in decidual tissue from RSA patients (**A–D**) and subjects undergoing healthy elective pregnancy termination (**E–H**). Single CD56^{+} cells are stained red (**arrowheads**), stathmin-1^{+}CD56^{+} cells are stained brown (**arrows**), and nuclei are stained blue with hematoxylin. Original magnification is marked. **B**, **D**, **F**, and **H** are local magnifications of the regions enclosed with boxes on **A**, **C**, **E**, and **G**, respectively. **I:** Mean density of stathmin-1^{+}CD56^{+} cells as determined using Image-Pro Plus 6.0. Error bars represent SD. $^{**}P < 0.01$.

stathmin-1^{+}DBA-lectin^{+} cells was significantly higher in CBA/J×BALB/c mice than in CBA/J×DBA/2J mice (Figure 5). Stathmin-1^{+}DBA-lectin^{+} cells were found mainly scattered in the decidua basalis and mesometrial lymphoid aggregate of pregnancy in the murine pregnant uteri. Because the decidua basalis and mesometrial lymphoid aggregate of pregnancy, to some extent, represent the maternal-fetal interface and because more immunopotent cells can infiltrate into these tissues than into other parts of murine placental and decidual tissues, these results suggest that stathmin-1^{+}DBA-lectin^{+} NK cells may be important in the modulation of maternal-fetal cross talk.[25,26] Similar results were obtained in human decidual tissue. Using CD56 as a pan-NK cell marker for human uNK cells, we found that the frequency of stathmin-1^{+}CD56^{+} cells was significantly higher in decidual tissues from normal early pregnancy than in those from spontaneous abortion patients (Figure 6). This suggests that some cases of unexplained spontaneous miscarriage may be attributable to reduced function of uNK cells, including reduced production of stathmin-1 protein in uNK cells. In addition, stathmin-1^{+}CD56^{+} cells were found mainly scattered in tissues near blood vessels, suggesting that they may participate in establishment, remodeling, or other functions of the blood vessel system. Stathmin-1^{+}CD56^{+} cells were less frequently detected in RSA samples, consistent with the results obtained using mouse two-color flow cytometry. Taken together, the results of the present study suggest that a fraction of uNK cells express stathmin-1 molecules and that insufficient stathmin-1 expression in uNK cells may be related to increased embryo loss in abortion-prone mice and some patients with RSA.

In addition to murine uNK cells, CD49b is also expressed by a small fraction of other cell types.[13] To our knowledge, there is not an ideal marker for murine uNK cells. A cell purification strategy using DBA-lectin and CD122 marker may be more specific for mouse uNK cell purification.[22] However, microbead-conjugated antibodies for DBA-lectin or CD122 are not commercially available. At present, microbead-conjugated anti-CD49b is used in MACS to purify uNK cells.[26] In future studies, it

would be helpful to exclude T cells and other cells by negative selection during uNK cell purification using microbead-conjugated CD3 and other antibodies specific for non-uNK cells that also express CD49b. Because B cells are virtually absent from the pregnant uterus, the possibility of B-cell contamination is small.[27] A recent report suggested that CD122 is a good marker for uNK cells.[22] To define the percentage of $CD122^+$ cells in the $CD49b^+$ population, we performed two-color flow cytometry using MACS-purified $CD49b^+$ cells stained with FITC-conjugated anti-CD122 and PE-conjugated anti-CD49b antibodies, which showed that most $CD49b^+$ cells were also positive for CD122 in CBA/J×DBA/2J and CBA/J×BALB/c mice.

Flow cytometry is quantitative by nature, allowing thousands of cells to be counted and objectively analyzed within minutes. Using two-color flow cytometry with cells stained by FITC-conjugated anti–stathmin-1 and PE-conjugated anti-CD49b, we confirmed that there are double-positive cells that express stathmin-1 and CD49b and determined the constitutional ratio of these cells. Stathmin-1 expression in $CD49b^+$ cells was also confirmed using MACS-purified $CD49b^+$ cells and proteomic assays in the present study (Figures 2 and 3).

In summary, decreased stathmin-1 expression in a murine abortion-prone model was confirmed using flow cytometry, 2-DE, MS, and Western blot analysis compared with normal fertile controls. In multivision IHC, colocalization of stathmin-1 and DBA-lectin was confirmed in both matings, but the frequency of stathmin-1^+DBA-lectin$^+$ cells was significantly lower in abortion-prone matings. Inhibition of stathmin-1 significantly boosted embryo resorption rates in mouse models. In patients who experience unexplained spontaneous abortion, the frequency of stathmin-1^+CD56^+ cells was also significantly lower than in normal pregnancy. These results suggest that adequate stathmin-1 expression in uNK cells may be critical to pregnancy success. In contrast, insufficient stathmin-1 expression may be correlated with pregnancy failure.

Acknowledgment

We thank Prof. Canrong Ni (Changhai Hospital, Shanghai, China) for his great help in multivision IHC.

References

1. Curmi PA, Gavet O, Charbaut E, Ozon S, Lachkar-Colmerauer S, Manceau V, Siavoshian S, Maucuer A, Sobel A: Stathmin and its phosphoprotein family: general properties, biochemical and functional interaction with tubulin. Cell Struct Funct 1999, 24:345–357
2. Rubin CI, Atweh GF: The role of stathmin in the regulation of the cell cycle. J Cell Biochem 2004, 93:242–250
3. Sobel A: Stathmin: a relay phosphoprotein for multiple signal transduction? Trends Biochem Sci 1991, 16:301–305
4. Brattsand G, Marklund U, Nylander K, Roos G, Gullberg M: Cell-cycle-regulated phosphorylation of oncoprotein 18 on ser16, ser25 and ser38. Eur J Biochem 1994, 220:359–368
5. Sobel A, Boutterin MC, Beretta L, Chneiweiss H, Doye V, Peyro-Saint-Paul H: Intracellular substrates for extracellular signaling: characterization of a ubiquitous, neuron-enriched phosphoprotein (stathmin). J Biol Chem 1989, 264:3765–3772
6. Tamura K, Yoshie M, Nishi H, Osakabe Y, Isaka K, Hara T, Kogo H: Expression of stathmin in human uterus and decidualizing endometrial stromal cells. Reproduction 2006, 132:625–636
7. Yoshie M, Tamura K, Kogo H: Differential localization of decidual stathmin during pregnancy in rats. Placenta 2004, 25:449–455
8. Tamura K, Hara T, Yoshie M, Irie S, Sobel A, Kogo H: Enhanced expression of uterine stathmin during the process of implantation and decidualization in rats. Endocrinology 2003, 144:1464–1473
9. Clark DA, Chaouat G, Arck PC, Mittruecker HW, Levy GA: Cytokine-dependent abortion in CBA × DBA/2 mice is mediated by the procoagulant fgl2 prothombinase. J Immunol 1998, 160:545–549
10. Redecha P, van Rooijen N, Torry D, Girardi G: Pravastatin prevents miscarriages in mice: role of tissue factor in placental and fetal injury. Blood 2009, 113:4101–4109
11. Lin Y, Wang H, Wang W, Zeng S, Zhong Y, Li D-J: Prevention of embryo loss in non-obese diabetic mice using adoptive $ITGA2^+ISG20^+$ natural killer-cell transfer. Reproduction 2009, 137:943–955
12. Lin Y, Zhong Y, Shen W, Chen Y, Shi J, Di J, Zeng S, Saito S: TSLP-induced placental DC activation and IL-10^+ NK cell expansion: comparative study based on BALB/c×C57BL/6 and NOD/SCID×C57BL/6 pregnant models. Clin Immunol 2008, 126:104–117
13. Barber EM, Pollard JW: The uterine NK cell population requires IL-15 but these cells are not required for pregnancy nor the resolution of a Listeria monocytogenes infection. J Immunol 2003, 171:37–46
14. Arase H, Saito T, Phillips JH, Lanier LL: The mouse NK cell-associated antigen recognized by DX5 monoclonal antibody is CD49b (α2 integrin, very late antigen-2). J Immunol 2001, 167:1141–1144
15. Lin Y, Zhong Y, Saito S, Chen Y, Shen W, Di J, Zeng S: Characterization of natural killer cells in nonobese diabetic/severely compromised immunodeficient mice during pregnancy. Fertil Steril 2009, 91:2676–2686
16. Lin Y, Liang Z, Chen Y, Zeng Y: TLR3-involved modulation of pregnancy tolerance in double-stranded RNA-stimulated NOD/SCID mice. J Immunol 2006, 176:4147–4154
17. Li C, Xiao Z, Chen Z, Zhang X, Li J, Wu X, Li X, Yi H, Li M, Zhu G, Liang S: Proteome analysis of human lung squamous carcinoma. Proteomics 2006, 6:547–558
18. Shen J, Pavone A, Mikulec C, Hensley SC, Traner A, Chang TK, Person MD, Fischer SM: Protein expression profiles in the epidermis of cyclooxygenase-2 transgenic mice by 2-dimensional gel electrophoresis and mass spectrometry. J Proteome Res 2007, 6:273–286
19. DiGiovanni J, Bol DK, Wilker E, Beltran L, Carbajal S, Moats S, Ramirez A, Jorcano J, Kiguchi K: Constitutive expression of insulin-like growth factor-1 in epidermal basal cells of transgenic mice leads to spontaneous tumor promotion. Cancer Res 2000, 60:1561–1570
20. Li C, Wang W, Wang H, Zhong Y, Di J, Lin Y: Proteomic analysis of proteins differentially expressed in uterine lymphocytes obtained from wild-type and NOD mice. J Cell Biochem 2009, 108:447–457
21. Lin Y, Zeng Y, Di J, Zeng S: Murine $CD200^+CK7^+$ trophoblasts in a poly (I: c)-induced embryo resorption model. Reproduction 2005, 130:529–537
22. Yadi H, Burke S, Madeja Z, Hemberger M, Moffett A, Colucci F: Unique receptor repertoire in mouse uterine NK cells. J Immunol 2008, 181:6140–6147
23. Alli E, Yang J-M, Ford JM, Hait WN: Reversal of stathmin-mediated resistance to paclitaxel and vinblastine in human breast carcinoma cells. Mol Pharmacol 2007, 71:1233–1240
24. Lin Y, Chen Y, Zeng Y, Wang T, Zeng S: Lymphocyte phenotyping and NK cell activity analysis in pregnant NOD/SCID mice. J Reprod Immunol 2005, 68:39–51
25. Croy BA, Chantakru S, Esadeg S, Ashkar AA, Wei Q: Decidual natural killer cells: key regulators of placental development. J Reprod Immunol 2002, 57:151–168
26. Wang W, Lin Y, Zeng S, Li D-J: Improvement of fertility with adoptive $CD25^+$ natural killer cell transfer in sub-fertile NOD mice. Reprod BioMed Online 2009, 18:95–103
27. von Rango U, Classen-Linke I, Kertschanska S, Kemp B, Beier HM: Effects of trophoblast invasion on the distribution of leukocytes in uterine and tubal implantation sites. Fertil Steril 2001, 76:116–124

J Epidemiol 2011;21(1):61-66
doi:10.2188/jea.JE20100092

Original Article

Smoking During Pregnancy Increases Risks of Various Obstetric Complications: A Case-Cohort Study of the Japan Perinatal Registry Network Database

Kunihiko Hayashi[1], Yoshio Matsuda[2], Yayoi Kawamichi[2], Arihiro Shiozaki[3], and Shigeru Saito[3]

[1]Department of Basic Medical Sciences, School of Health Sciences, Faculty of Medicine, Gunma University, Gunma, Japan
[2]Department of Obstetrics and Gynecology, Tokyo Women's Medical University, Tokyo, Japan
[3]Department of Obstetrics and Gynecology, Faculty of Medicine, University of Toyama, Toyama, Japan

Received June 11, 2010; accepted September 14, 2010; released online November 13, 2010

ABSTRACT

Background: The adverse effects of maternal smoking on the health of pregnant women have been examined mostly on a disease-by-disease basis. The aims of this study were to evaluate simultaneously the effects of smoking during pregnancy on various obstetric complications, using data from a large medical database, and to investigate the expediency of using a case-cohort design for such an analysis.

Methods: A case-cohort study was conducted within the Japan Perinatal Registry Network database. Perinatal information on infant deliveries was entered into the database at 125 medical centers in Japan. The base population of the study was 180 855 pregnant women registered in the database from 2001 through 2005. The outcome measures were the incidences of 11 different obstetric complications. Logistic regression models were used to estimate age-adjusted risk ratios (aRRs) and relative excess incidence proportions (REIs).

Results: The overall prevalence of smoking during pregnancy was 5.8% in the base cohort, and the prevalence was higher among younger women. A comparison of the cases and control cohort showed that smokers during pregnancy had statistically significant higher risks for preterm rupture of the membrane (aRR: 1.67, 95% confidence interval [CI]: 1.43–1.96; REI: 40.2%, 95% CI: 29.9%–49.1%), chorioamnionitis (1.65, 1.36–2.00; 39.4%, 26.4%–50.0%), incompetent cervix (1.63, 1.35–1.96; 38.5%, 25.8%–49.1%), threatened premature delivery (1.38, 1.17–1.64; 27.7%, 14.5%–38.9%), placental abruption (1.37, 1.10–1.72; 27.1%, 8.8%–41.7%), and pregnancy-induced hypertension (1.20, 1.01–1.41; 16.4%, 1.2%–29.3%).

Conclusions: Maternal smoking was associated with a number of obstetric complications. This highlights the importance of smoking cessation during pregnancy. In addition, case-cohort analysis proved useful in estimating RRs for multiple outcomes in a large database.

Key words: smoking during pregnancy; obstetric complications; perinatal epidemiology; case-cohort study; registry database

INTRODUCTION

According to the Organisation for Economic Co-operation and Development (OECD), the prevalence of current smoking in adult women is 13% in Japan, 14% in the United States, 19% in Germany, and 20% in the United Kingdom.[1] Although many pregnant women try to quit smoking, and some tobacco control programs have successfully reduced the proportion of smoking mothers,[2] the prevalence of smoking during pregnancy is approximately 6.5% in Japan,[3,4] 12% in the United States,[5] 12% in Germany,[6] and 15% in the United Kingdom.[7]

The adverse effects of maternal smoking during pregnancy on the health of a fetus are well known and include still births, fetal growth restriction, decreased infant birth weight, and neonatal death. In addition, pregnant women who smoke may themselves experience complications such as premature rupture of the amniotic membrane. However, there are no comprehensive evaluations of the adverse effects of smoking on the health of pregnant women, because many different obstetric complications are possible and most studies examine these complications individually.

A case-cohort study—which is identical to a case-base design in which the base cohort is closed and the measure of

Address for correspondence. Kunihiko Hayashi, PhD, Department of Basic Medical Sciences, School of Health Sciences, Faculty of Medicine, Gunma University, 3-39-15 Showa-machi, Maebashi, Gunma 371-8514, Japan (e-mail: khayashi@health.gunma-u.ac.jp).
Copyright © 2010 by the Japan Epidemiological Association

interest is an incidence proportion rather than an incidence rate—is a variation of the case-control design in which the controls are drawn from the entire base population, regardless of their disease status.[8–10] These conditions for the base cohort in a case-cohort design are common in perinatal epidemiologic studies.[9,10] We evaluated the adverse effects of smoking during pregnancy on 11 different obstetric complications, using a population-based database, and examined the expediency of using a case-cohort design for such a comprehensive evaluation.

METHODS

Study design and data source

We conducted a case-cohort study using the Japan Perinatal Registry Network database, which was started in 1974 and is managed by the Japan Society of Obstetrics and Gynecology. This database was converted to its present database structure in 2001. It includes all live and stillbirths at 125 medical centers in Japan, including 76 university hospitals, 14 national hospitals, 10 Japanese Red Cross hospitals, and 25 other hospitals, and covered 5.2% (56 671 registered births) of the total 1 094 434 live and stillbirths in Japan in 2005.

A detailed description of the database has been published elsewhere.[11] In brief, a self-administered questionnaire, interview, and medical records were used to collect information on maternal age, parity, cigarette smoking during pregnancy, alcohol intake during pregnancy, medical history, history of treatment for infertility, major obstetric complications during pregnancy, mode of delivery, and neonatal outcomes. Data entry was routinely performed by attendants at the time of delivery. The data conform to uniform coding specifications and diagnostic criteria for complications and were subject to rigorous quality checking. Smoking during pregnancy and the incidence of each obstetric complication were coded as "yes" or "no" in the database. The dataset for the study was provided by the Japan Society of Obstetrics and Gynecology. The study protocol was reviewed and approved by the ethics committee of Tokyo Women's Medical University.

The base cohort of the study consisted of 180 855 pregnant women carrying a singleton fetus who were registered in the database from 2001 through 2005. Complete information on obstetric complications and smoking status during pregnancy was present for all women included in the base cohort.

Case identification and control selection

From the base cohort, the cases were independently identified for 11 obstetric complications: threatened premature delivery before 37 completed weeks of pregnancy, incompetent cervix, pregnancy-induced hypertension, eclampsia, pulmonary edema, placental abruption, placenta previa, preterm premature rupture of the membrane (PROM) before 37 completed weeks of pregnancy, chorioamnionitis, placenta accreta, and disseminated intravascular coagulation syndrome.

The procedures for control selection in a conventional nested case-control study and a case-cohort study are illustrated schematically in Figure 1. To perform a comprehensive evaluation of multiple outcomes using a large database, a case-cohort study is preferable to a conventional nested case-control study, which is the most common study design.[10] An advantage of the case-cohort design is that it allows the use of the same controls (ie, a subcohort selected from the base cohort) for several different outcome diseases. The control cohort in the current case-cohort study was selected randomly from the entire base cohort and included both cases and non-cases. We selected 3749 women for the control cohort, which represented at least 2% of all registered pregnant women in each hospital. The same control cohort was used in the analysis of each obstetric complication.

Statistical analysis

Unconditional logistic regression models were used to estimate ratios of incidence proportions (risk ratios, RRs) and 95% confidence intervals (CIs) for the association of smoking during pregnancy with the incidence of each obstetric complication. The RR is estimated from the ratio of pseudo-risks by sampling controls from subjects at risk in a case-cohort design, and the incidence odds ratio (OR) is estimated by sampling from non-cases in a cumulative case-control study.[9] We conducted a case-cohort comparison; therefore, logistic regression analysis provided an exact estimate of the RR without any arguments on a rare-disease assumption for outcome events. It is often assumed that the outcome disease under study is rare when the incidence OR approximates the RR. In general, this assumption is not needed, however, even in a case-control study. However, the incidence OR in a case-control study is not expected to be a good approximation of the RR, unless the incidence proportion is less than approximately 0.1.[9]

Smoking is one of the most preventable risk factors. For that reason, relative excess incidence proportions (REIs), which are identical to attributable fractions in the exposed population, and 95% CIs were calculated using the exact estimate of RRs:

$$\text{REI}\ (\%) = \frac{\text{RR} - 1}{\text{RR}} \times 100$$

The REI is the fraction of the obstetric complication burden among smokers during pregnancy that would not have occurred if the smokers had the same incidence of complications as nonsmokers during pregnancy.[12]

Wald's χ^2 test was performed in the logistic regression analysis, and $P < 0.05$ was considered statistically significant. All statistical data analyses were carried out using SAS ver. 9.1 (SAS Institute Inc., Cary, NC, USA).

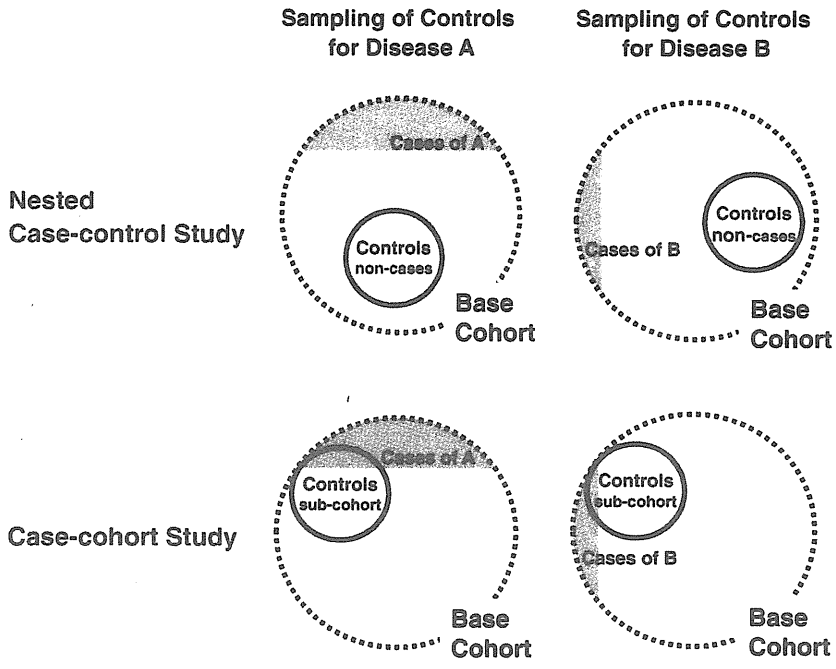

Figure 1. Control selection in nested case-control and case-cohort studies

RESULTS

Smoking during pregnancy in base cohort

The base cohort included 180 855 women. At the time of delivery, 2834 (1.6%) of the women were younger than 20 years, 17 867 (9.9%) were 20 to 24 years of age, 54 057 (29.9%) were 25 to 29 years of age, 67 886 (37.5%) were 30 to 34 years of age, 32 173 (17.8%) were 35 to 39 years of age, and 6038 (3.3%) were 40 years or older.

A total of 10 527 women (5.8%) in the base cohort smoked during pregnancy. The prevalence of smoking during pregnancy tended to gradually increase as maternal age decreased. In particular, the prevalence of smoking during pregnancy was high in women younger than 20 years (15.7%) and in women aged 20 to 24 years (10.7%), as shown in Table 1.

Table 1. Prevalence of smoking during pregnancy in base cohort

	Prevalence	No. of smokers		No. of women
All women	5.8%	10 527	/	180 855
Maternal age at delivery, years				
≤19	15.7%	444	/	2834
20–24	10.7%	1910	/	17 867
25–29	5.8%	3136	/	54 057
30–34	4.7%	3166	/	67 886
35–39	4.8%	1545	/	32 173
≥40	5.4%	326	/	6038

Cases of obstetric complications identified in base cohort

In the base cohort, we identified 5681 cases (incidence proportion 3.14%) of threatened premature delivery before 37 completed weeks of pregnancy, 2943 cases (1.63%) of incompetent cervix, 7371 cases (4.08%) of pregnancy-induced hypertension, 143 cases (0.08%) of eclampsia, 76 cases (0.04%) of pulmonary edema, 1770 cases (0.98%) of placental abruption, 2369 cases (1.31%) of placenta previa, 6902 cases (3.82%) of preterm PROM before 37 completed weeks of pregnancy, 2508 cases (1.39%) of chorioamnionitis, 202 cases (0.11%) of placenta accreta, and 343 cases (0.19%) of disseminated intravascular coagulation syndrome.

Effect of maternal smoking on obstetric complications

A total of 216 women (5.8%) in the control cohort smoked during pregnancy. The prevalence of smoking during pregnancy in the identified cases is shown in Table 2. The crude ratios of incidence proportions (crude RRs) of smoking were statistically significant for threatened premature delivery before 37 completed weeks of pregnancy, incompetent cervix, placental abruption, preterm PROM before 37 completed weeks of pregnancy, and chorioamnionitis. The estimates of ratios of incidence proportions adjusted by maternal age at delivery (age-adjusted RR) are also shown in Table 2. Maternal smoking during pregnancy was significantly associated with threatened premature delivery before 37 completed weeks of pregnancy (age-adjusted RR 1.38), incompetent cervix (1.63), pregnancy-induced hypertension (1.20), placental abruption

Table 2. Prevalence of smoking during pregnancy, and risk ratios (RRs) and relative excess incidence proportions (REIs) for obstetric complications

	Smoking prevalence	Crude RR (95% CI)	Age-adjusted RR (95% CI)	Age-adjusted REI[a] (95% CI)
Control cohort	5.8%			
Cases of obstetric complications				
Threatened premature delivery[b]	8.0%	1.42 (1.20–1.68)	1.38 (1.17–1.64)	27.7% (14.5%–38.9%)
Incompetent cervix	8.8%	1.58 (1.31–1.90)	1.63 (1.35–1.96)	38.5% (25.8%–49.1%)
Pregnancy-induced hypertension	6.5%	1.14 (0.97–1.35)	1.20 (1.01–1.41)	16.4% (1.2%–29.3%)
Eclampsia	4.9%	0.84 (0.39–1.82)	0.82 (0.38–1.78)	
Pulmonary edema	6.6%	1.15 (0.46–2.88)	1.22 (0.49–3.06)	
Placental abruption	7.6%	1.34 (1.07–1.67)	1.37 (1.10–1.72)	27.1% (8.8%–41.7%)
Placenta previa	5.6%	0.97 (0.77–1.21)	1.07 (0.85–1.34)	
Preterm PROM[b]	9.3%	1.68 (1.43–1.97)	1.67 (1.43–1.96)	40.2% (29.9%–49.1%)
Chorioamnionitis	9.3%	1.68 (1.38–2.03)	1.65 (1.36–2.00)	39.4% (26.4%–50.0%)
Placenta accreta	7.9%	1.41 (0.83–2.39)	1.52 (0.89–2.59)	
DIC syndrome	7.3%	1.29 (0.84–1.98)	1.35 (0.88–2.08)	

CI. confidence interval; DIC: disseminated intravascular coagulation; PROM: premature rupture of the membranes.
[a]REI was calculated for obstetric complications significantly associated with maternal smoking during pregnancy.
[b]Before 37 weeks of pregnancy.

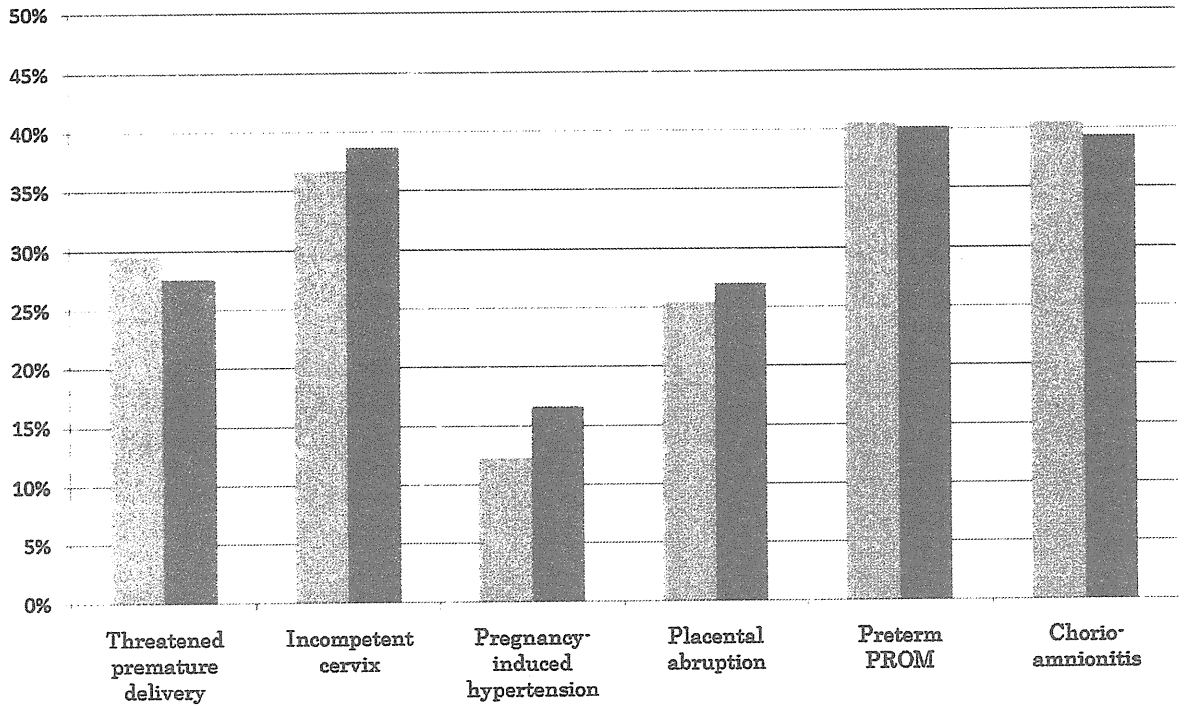

Figure 2. Relative excess incidence proportion (REI) of obstetric complications associated with smoking during pregnancy (left bars: crude REI, right bars: age-adjusted REI)

(1.37), preterm PROM before 37 completed weeks of pregnancy (1.67), and chorioamnionitis (1.65).

As for obstetric complications significantly associated with maternal smoking during pregnancy, crude and age-adjusted REIs are shown in Figure 2. The figure includes both crude and age-adjusted REI for pregnancy-induced hypertension, although the crude association was not statistically significant. Among smoking women, the age-adjusted REIs for threatened premature delivery before 37 completed weeks of pregnancy, incompetent cervix, pregnancy-induced hypertension, placental abruption, preterm PROM before 37 completed weeks of pregnancy, and chorioamnionitis were 27.7%, 38.5%, 16.4%, 27.1%, 40.2%, and 39.4%, respectively (Figure 2, Table 2).

DISCUSSION

Effects of maternal smoking on pregnancy-related complications

We found a statistically significant association between

maternal smoking and the incidence of 6 of 11 obstetric complications. Obstetric complications may share many risk factors, of which maternal smoking appears to be one of the most relevant. Previous studies have reported similar adverse effects of maternal smoking on preterm PROM (OR 1.25 to 2.5),[13–15] chorioamnionitis (bacterial vaginosis; OR 1.72),[16] threatened premature delivery (OR 1.34 and 1.3),[13,17] and placental abruption (OR 1.62 to 2.05).[15,18–20] However, to the best of our knowledge, no other epidemiologic study has shown an association between maternal smoking and incompetent cervix, which was the fourth most common obstetric complication in the base cohort of the current study. This newly discovered association with maternal smoking deserves greater attention.

There is controversy regarding the effect of smoking on pregnancy-induced hypertension. Some studies have reported a large reduction in the risk of pregnancy-induced hypertension with maternal smoking (ORs of 0.6 and 0.80 for primiparous women[21] and 0.81 for multiparous women)[22]; other studies have reported a statistically nonsignificant change (OR 1.1)[23] or a strong positive association.[24] We observed a slight increase in the risk of pregnancy-induced hypertension in smokers: the aRR was 1.20, which lies between the values noted in other studies. It is possible that the effect size in different studies varies according to other risk factors, such as chronic hypertension.

Eclampsia was the only obstetric event for which the risk was lower among women who smoked (aRR 0.82), although this decrease was not statistically significant. Other studies have also shown that smoking decreases the incidence of eclampsia (ORs of 0.7,[25] and 0.74 for primiparous women and 0.75 for multiparous women).[22]

Expediency of case-cohort design

The present case-cohort design was useful for comprehensively evaluating the risk of multiple outcomes associated with maternal smoking. Only 1 control subcohort was required for the analyses of 11 different obstetric complications. In contrast, if we had applied a nested case-control design, 11 different control groups would have been needed. Although we could have selected this 1 control group from subjects who were completely free from all 11 obstetric complications in a case-control study, this would have led to significant selection bias, as there are many common risk factors for the complications we studied. The subjects exposed to these common risk factors would have been systematically excluded if we had included only subjects free of complications. Such bias does not occur in a case-cohort design.

The case-cohort design was also advantageous in estimating REIs in the present study. The estimated RRs were relatively small: the largest aRR was 1.67 for preterm rupture of the membrane. REI is by definition more sensitive to a change in the estimated RR when the RR is closer to 1. In such a situation, the fact that case-cohort analyses provide an exact estimate of the RR, without the need for an approximation, made it possible for us to estimate accurate REIs.

Methodological strengths and limitations of the study

Many studies have shown an effect of maternal smoking on a single obstetric complication. Such a disease-by-disease approach cannot distinguish between disease-specific variations and study-specific variations. However, the current case-cohort study revealed the adverse effects of maternal smoking on multiple complications.

This study does have some limitations. First, we could not examine the effect of smoking after adjusting for potential socioeconomic confounders because information on socioeconomic status was not available in the database. Second, smoking status during pregnancy was self-reported on questionnaires and in interviews. This type of information gathering likely underestimates the prevalence of pregnant smokers, because not all women will report their smoking[26] and because smokers who quit during pregnancy tend to describe themselves as nonsmokers. This underestimation of smokers leads to potential underestimation of the effect size of smoking. Third, the database has no information on the number of cigarettes smoked daily. Therefore we could not examine any dose-response relationship between smoking and the incidences of obstetric complications.

Conclusions

Maternal smoking was associated with a number of obstetric complications in a case-cohort analysis of a large perinatal registry database. The study highlighted the importance of smoking cessation during pregnancy. In addition, the case-cohort design proved useful in estimating relative risks for multiple outcomes in a large medical database.

ACKNOWLEDGMENTS

This work was supported in part by the Japan Ministry of Health, Labour and Welfare [H20-Kodomo Research Grant on Children and Families]. The authors thank Norio Sugimoto for his assistance with data management and analysis.

Conflicts of interest: None declared.

REFERENCES

1. Organisation for Economic Co-operation and Development (OECD). Health at a glance 2009: OECD Indicators. Paris: OECD Publishing; 2009. Available from: http://dx.doi.org/10.1787/health_glance-2009-en.
2. Stein CR, Ellis JA, Savitz DA, Vichinsky L, Perl SB. Decline in smoking during pregnancy in New York City, 1995–2005. Public Health Rep. 2009:124(6):841–9.
3. Takimoto H, Yoshiike N, Katagiri A, Ishida H, Abe S. Nutritional status of pregnant and lactating women in Japan: a

comparison with non-pregnant/non-lactating controls in the National Nutrition Survey. J Obstet Gynaecol Res. 2003;29(2):96–103.
4. Suzuki K, Tanaka T, Kondo N, Minai J, Sato M, Yamagata Z. Is maternal smoking during early pregnancy a risk factor for all low birth weight infants? J Epidemiol. 2008;18(3):89–96.
5. Tong VT, Jones JR, Dietz PM, D'Angelo D, Bombard JM. Trend in smoking before, during, and after pregnancy: Pregnancy Risk Assessment Monitoring System (PRAMS), United States, 31 sites, 2000–2005. MMWR Surveill Summ. 2009;58(4):1–29.
6. Meyer S, Raisig A, Gortner L, Ong MF, Bücheler M, Tutdibi E. In utero tobacco exposure: the effects of heavy and very heavy smoking on the rate of SGA infants in the Federal State of Saarland, Germany. Eur J Obstet Gynecol Reprod Biol. 2009;146(1):37–40.
7. Crozier SR, Robinson SM, Borland SE, Godfrey KM, Cooper C, Inskip HM; SWS Study Group. Do women change their health behaviours in pregnancy? Findings from the Southampton Women's Survey. Paediatr Perinat Epidemiol. 2009;23(5):446–53.
8. Miettinen O. Design options in epidemiologic research: An update. Scand J Work Environ Health. 1982;8 Suppl 1:7–14.
9. Rothman KJ, Greenland S, Lash TL. Modern epidemiology. 3rd ed. Philadelphia: Lippincott Williams & Wilkins; 2008. p. 113–25.
10. Wacholder S. Practical considerations in choosing between the case-cohort and nested case-control designs. Epidemiology. 1991;2(2):155–8.
11. Matsuda Y, Hayashi K, Shiozaki A, Kawamichi Y, Satoh S, Saito S. Comparison of risk factors for placental abruption and placenta previa. J Obstet Gynaecol Res. In press.
12. Walker AM. Observation and inference: An introduction to the methods of epidemiology. Chestnut Hill, MA: Epidemiology Resources Inc.; 1991. p. 15–25.
13. Nabet C, Lelong N, Ancel PY, Saurel-Cubizolles MJ, Kaminski M. Smoking during pregnancy according to obstetric complications and parity: results of EUROPOP study. Eur J Epidemiol. 2007;22:715–21.
14. Burguet A, Kaminski M, Abraham-Lerat L, Schaal JP, Cambonie G, Fresson J, et al; EPIPAGE Study Group. The complex relationship between smoking in pregnancy and very preterm delivery. Results of Epipage study. BJOG. 2004;111:258–65.
15. Castles A, Adams EK, Melvin CL, Kelsch C, Boulton ML. Effects of smoking during pregnancy. Five meta-analyses. Am J Prev Med. 1999;16(3):208–15.
16. Svare JA, Schmidt H, Hansen BB, Lose G. Bacterial vaginosis in a cohort of Danish pregnant women: prevalence and relationship with preterm delivery, low birth weight and perinatal infections. BJOG. 2006;113:1419–25.
17. McPheeters ML, Miller WC, Hartmann KE, Savitz DA, Kaufman JS, Garrett JM, et al. The epidemiology of threatened preterm labor: a prospective cohort study. Am J Obstet Gynecol. 2005;192(4):1325–9.
18. Ananth CV, Savitz DA, Luther ER. Maternal cigarette smoking as a risk factor for placental abruption, placenta previa, and uterine bleeding in pregnancy. Am J Epidemiol. 1996;144(9):881–9.
19. Mortensen JT, Thulstrup AM, Larsen H, Møller M, Sørensen HT. Smoking, sex of offspring, and risk of placental abruption, placenta previa, and preeclampsia: a population-based cohort study. Acta Obstet Gynecol Scand. 2001;80(10):894–8.
20. Tikkanen M, Nuutila M, Hiilesmaa V, Paavonen J, Ylikorkala O. Clinical presentation and risk factors of placental abruption. Acta Obstet Gynecol Scand. 2006;85(6):700–5.
21. Zhang J, Klebanoff MA, Levine RJ, Puri M, Moyer P. The puzzling association between smoking and hypertension during pregnancy. Am J Obstet Gynecol. 1999;181(6):1407–13.
22. Yang Q, Wen SW, Smith GN, Chen Y, Krewski D, Chen XK, et al. Maternal cigarette smoking and the risk of pregnancy-induced hypertension and eclampsia. Int J Epidemiol. 2006;35(2):288–93.
23. Villar J, Carroli G, Wojdyla D, Abalos E, Giordano D, Ba'aqeel H, et al. Preeclampsia, gestational hypertension and intrauterine growth restriction, related or independent conditions? Am J Obstet Gynecol. 2006;194(4):921–31.
24. Bakker R, Steegers EA, Mackenbach JP, Hofman A, Jaddoe VW. Maternal smoking and blood pressure in different trimesters of pregnancy. The Generation R Study. J Hypertens.. 2010;28(11):2210–8.
25. Roelands J, Jamison MG, Lyerly AD, James AH. Consequences of smoking during pregnancy on maternal health. J Womens Health (Larchmt). 2009;18(6):867–72.
26. Shipton D, Tappin DM, Vadiveloo T, Crossley JA, Aitken DA, Chalmers J. Reliability of self reported smoking status by pregnant women for estimating smoking prevalence: a retrospective, cross sectional study. BMJ. 2009;339:b4347.

EMBO reports

scientific report

RodZ regulates the post-transcriptional processing of the *Shigella sonnei* type III secretion system

Jiro Mitobe[1+], *Itaru Yanagihara*[2], *Kiyouhisa Ohnishi*[2], *Shouji Yamamoto*[1], *Makoto Ohnishi*[1], *Akira Ishihama*[3] & *Haruo Watanabe*[1]

[1]Department of Bacteriology I, National Institute of Infectious Diseases, Tokyo, [2]Department of Developmental Medicine, Research Institute, Osaka Medical Center for Maternal and Child Health, Osaka, and [3]Department of Frontier Bioscience, Hosei University, Tokyo, Japan

The expression of the type III secretion system—a main determinant of virulence in *Shigella*—is controlled by regulator cascades VirF-InvE (VirB) and CpxAR two-component system. A screen for mutants that restore virulence in the *cpxA* background led to the isolation of a mutant of *rodZ*, a cytoskeletal protein that maintains the rod-shaped morphology of bacilli. InvE is normally repressed at 30 °C because of decreased messenger RNA (mRNA) stability, but *rodZ* mutants markedly increase *invE*-mRNA stability. Importantly, the inhibition of InvE production by RodZ can be genetically separated from its role in cell-shape maintenance, indicating that these functions are distinguishable. Thus, we propose that RodZ is a new membrane-bound RNA-binding protein that provides a scaffold for post-transcriptional regulation.

Keywords: bacterial cytoskeleton; post-transcriptional regulation; *Shigella*; type III secretion system

EMBO *reports* (2011) 12, 911–916. doi:10.1038/embor.2011.132

INTRODUCTION

Recent studies of the regulation of bacterial cell-shape have shown that a set of bacterial cytoskeletal proteins maintain the rod-shaped morphology of bacilli. *Escherichia coli* MreB is a cytoskeletal protein that polymerizes into filaments—similarly to eukaryotic actin—that form helical arrays within the bacterial cytosol (Jones *et al*, 2001). Recently, RodZ (YfgA) was identified as a putative cytoskeletal anchoring protein that colocalizes with MreB at the inner membrane. Mutants of *rodZ* with altered cell morphology were isolated by microscopic screening of a collection of non-essential gene deletion mutants in *E. coli* K-12 (Shiomi *et al*, 2008), analysis of a transposon library from *Caulobacter crescentus* (Alyahya *et al*, 2009) and screening of *E. coli* K-12 mutants that require excess amounts of the cell-division protein FtsZ for growth on rich media (Bendezu *et al*, 2009). MreB and RodZ interact to define the long and short axes of *E. coli*.

A new *rodZ* mutant was identified in *Shigella sonnei*, an organism closely related to *E. coli*. Clinically, *Shigella* invades and propagates within the epithelial cells of the human intestine, resulting in the onset of bloody diarrhoea. The pathogenesis of *Shigella* is mediated by the type III secretion system (TTSS) encoded on the virulence plasmid that injects effector molecules into the host epithelium during infection (Dorman & Porter, 1998). Expression of the TTSS is tightly regulated by two proteins, VirF and InvE. VirF—an AraC-type transcriptional regulator—activates the transcription of *invE* (*virB*; Adler *et al*, 1989; Kato *et al*, 1989), and InvE—a homologue of the plasmid-partitioning factor ParB (Watanabe *et al*, 1990)—activates transcription of *mxi-spa* and *ipa* genes that encode the components of the TTSS (Beloin & Dorman, 2003).

The TTSS supports bacterial survival by repressing unnecessary expression under adverse conditions, such as low temperature (Maurelli *et al*, 1984) and low osmotic-pressure (Porter & Dorman, 1994). Repression is primarily accomplished through the post-transcriptional regulation of *invE* messenger RNA (mRNA). At a permissive temperature of 37 °C, *invE*-mRNA is stable, but its stability markedly decreases at 30 °C or under low osmotic-pressure. The deletion of *hfq*, an important RNA chaperone that is involved in the post-transcriptional regulation of many genes, leads to the recovery of *invE*-mRNA stability and increased TTSS gene expression (Mitobe *et al*, 2008, 2009).

Expression of TTSS is also under the control of the CpxAR two-component system (Nakayama & Watanabe, 1998). Transcription of *virF* depends on the phosphorylated form of the response regulator CpxR, which suggests a functional hierarchy: CpxAR > VirF > InvE. In the *cpxA* mutant, however, transcription of *invE* is maintained because *virF* is transcribed by autophosphorylated CpxR, as is the case for other Cpx-regulated genes (Alves *et al*, 2003). Although *invE*-mRNA is transcribed, the corresponding amount of InvE protein is not synthesized in the *cpxA* mutant at the permissive temperature of 37 °C (Mitobe *et al*, 2005).

[1]Department of Bacteriology I, National Institute of Infectious Diseases, Shinjuku, Tokyo 162-8640,
[2]Department of Developmental Medicine, Research Institute, Osaka Medical Center for Maternal and Child Health, Izumi, Osaka 594-1101,
[3]Department of Frontier Bioscience, Hosei University, Koganei, Tokyo 184-8584, Japan
[+]Corresponding author. Tel: +81 35 285 1111/ext. 2228; Fax: +81 35 285 1161; E-mail: jmitobe@nih.go.jp

Received 24 November 2010; revised 13 June 2011; accepted 14 June 2011; published online 22 July 2011

©2011 EUROPEAN MOLECULAR BIOLOGY ORGANIZATION

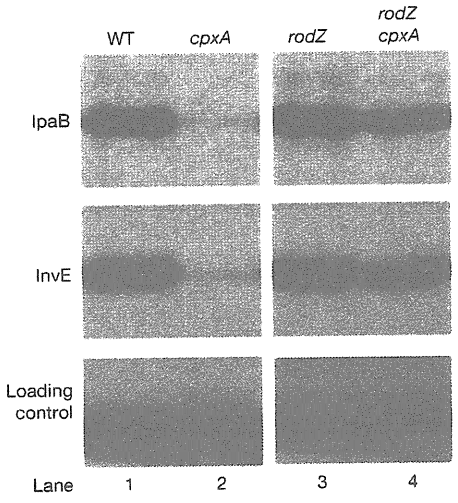

Fig 1 | Type III secretion system-encoding gene expression in *Echerichia coli* strains carrying a virulence plasmid from *Shigella sonnei*. Immunoblot analysis of IpaB and InvE expression at 37 °C. A nonspecific protein that cross-reacted with the InvE antibody (lower panel) was used as a loading control throughout the study. Lanes: 1, HW1273 (WT); 2, ME2824 (Δ*cpxA*); 3, ME5201 (Δ*rodZ*); 4, ME5199 (Δ*cpxA*/Δ*rodZ*). WT, wild type.

To elucidate the mechanism for this, a mutant that expressed InvE-regulated TTSS genes was isolated under the *cpxA* mutant background. The transposon was unexpectedly found to map to the locus encoding bacterial cytoskeleton RodZ.

RESULTS AND DISCUSSION

Isolation of a *rodZ* mutant

A *cpxA*-sensor deletion mutant showed reduced expression of InvE, as well as the TTSS effector molecule IpaB, at 37 °C (Fig 1A, lane 2). The reduction in *invE* expression was caused by a defect in post-transcriptional processing (Mitobe *et al*, 2005). To investigate this repression mechanism, secondary mutations that caused recovery of TTSS expression in the *cpxA* mutant background were identified. A *cpxA*-deletion mutant of *E. coli* (strain ME2824) that carried a reporter plasmid encoding a TTSS(*mxiC*)–*lacZ* fusion gene (pJM1718) was constructed and subjected to Tn*5* transposon mutagenesis. After screening 2×10^4 colonies, a single Tn*5*-transposon-insertion mutant was isolated that exhibited enhanced β-galactosidase activity. The Tn*5* insertion site was mapped to 11 base-pairs downstream from the amino-terminal end of the *rodZ* (*yfgA*) gene (see supplementary information online) that encodes a new bacterial cytoskeletal protein involved in the maintenance of cell shape. To confirm the involvement of RodZ in TTSS expression, a deletion mutant (*cpxA*/*rodZ*, ME5199) was constructed that produced wild-type levels of InvE and IpaB at 37 °C (Fig 1, lane 4). This showed that RodZ was involved in CpxA-dependent expression of TTSS-related genes. The amount of RodZ protein increased slightly in the parental *cpxA* mutant, and deletion of the response regulator *cpxR* or both of the *cpxRA* genes had no effect on the expression of a *rodZ–lacZ* reporter gene (supplementary Fig S1A,B online). Therefore, the CpxAR two-component system probably does not directly regulate transcription of the *rodZ* gene.

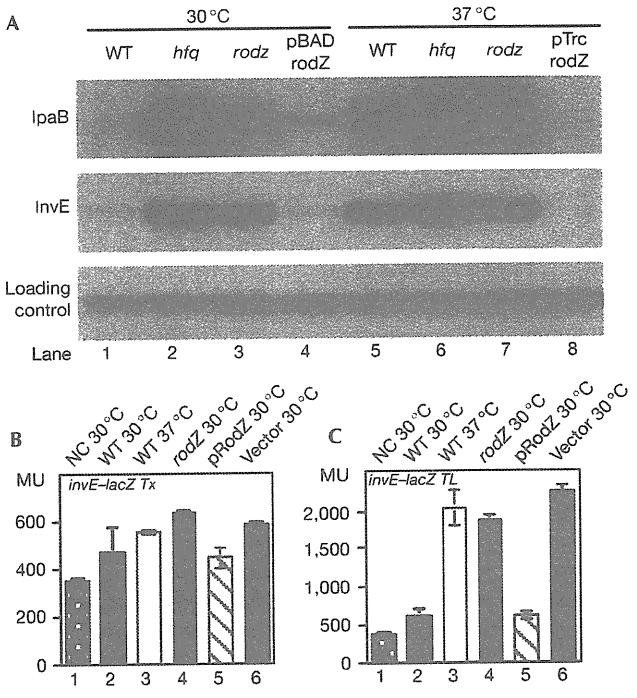

Fig 2 | Type III secretion system-encoding gene expression in *Shigella sonnei*. (A) Immunoblot analysis of IpaB and InvE at 30 °C (lanes 1–4) and 37 °C (lanes 5–8). Lanes: 1 and 5, MS390 (WT); 2 and 6, MS4831 (Δ*hfq*); 3 and 7, MS5201 (Δ*rodZ*); lane 4, MS5201 carrying pBAD-rodZ; lane 8, MS5201 carrying pTrc-rodZ. (B) β-galactosidase activity of an *invETx–lacZ* transcriptional fusion reporter protein (pJM4320). (C) β-galactosidase activity of an *invETL–lacZ* translational fusion reporter protein (pJM4321). (B,C) Bars: 1, MS506 (NC, avirulent *S. sonnei*); 2, MS390 (WT *S. sonnei*); 3, MS390 at 37 °C; 4, MS5201 (Δ*rodZ*); 5, MS5201 (Δ*rodZ*) MS5201 carrying pBAD-rodZ; 6, MS5201 carrying pBAD18Kan. Error bars represent s.d. of four independent experiments. MU, Miller units; NC, negative control; WT, wild type.

Expression of *invE* in *rodZ* mutants

To determine the regulatory role of RodZ, the *rodZ* deletion mutation was introduced into wild-type *S. sonnei*. The expression of *invE* is normally repressed at 30 °C (Fig 2A, lane 1), but repression is abolished in an *hfq* deletion mutant (Fig 2A, lane 2) that is involved in the post-transcriptional control of *invE*-mRNA (Mitobe *et al*, 2008). Similarly to the *hfq* mutant, robust expression of InvE and IpaB proteins was detected in the *rodZ* mutant strain (MS5201) at 30 °C (Fig 2A, lane 3). Expression of Hfq and RodZ were mutually independent because the amounts of the corresponding proteins were not affected in the respective *rodZ* and *hfq* mutants (supplementary Fig 1C online). The copy number of the virulence plasmid—which was measured by real-time PCR to detect the *invE* gene—was unaffected in either mutant (see supplementary information online). Expression of RodZ in the *rodZ* mutant with the pBAD-rodZ plasmid repressed expression of InvE and IpaB at 30 °C (Fig 2A, lane 4), but not at 37 °C (data not shown). Overexpression of RodZ with pTrc-rodZ repressed InvE and IpaB expression, even at 37 °C (Fig 2A, lane 8).

Transcription of the *invE* gene was measured using the *lacZ* reporter plasmid. In wild-type *S. sonnei*, the β-galactosidase

©2011 EUROPEAN MOLECULAR BIOLOGY ORGANIZATION

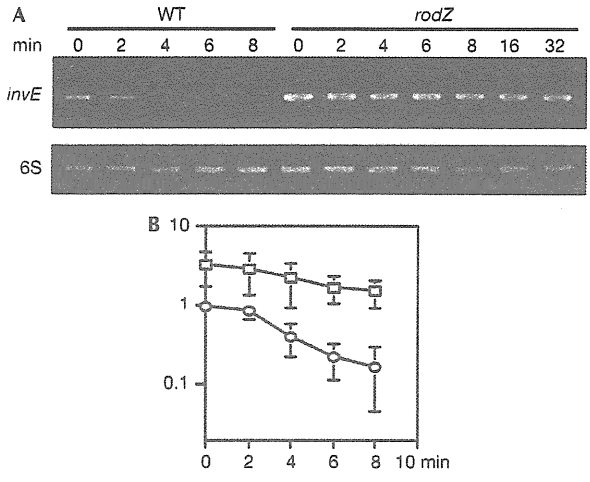

Fig 3 | Stability of *invE*-messenger RNA. (A) Reverse transcription-PCR of *invE*-mRNA using 6S RNA as a control. Minutes indicate the time after rifampicin treatment. WT, *Shigella sonnei* strain MS390; *rodZ*, strain MS5201 (Δ*rodZ*). **(B)** Real-time PCR of *invE*-mRNA in wild-type *S. sonnei* (MS390, circles) and Δ*rodZ* (MS5201, squares). mRNA was normalized to 6S RNA. Values relative to the wild type at time 0 are plotted on the semilog plot. Error bars represent s.d. of four independent experiments. mRNA, messenger RNA; WT, wild type.

activity directed by the *invE–lacZ* transcriptional fusion was almost the same at the non-permissive and permissive temperatures, 30 and 37 °C, respectively. This is different from the activity measured using the *invE–lacZ* translational fusion, in which β-galactosidase activity was lower at 30 °C (Fig 2B,C). Thus, the temperature-dependent repression of *invE* expression in wild-type *S. sonnei* occurs at the post-transcriptional level.

In the *rodZ* mutant, the β-galactosidase activity driven by the *invE–lacZ* transcriptional fusion was similar to that of the wild-type strain or the *rodZ* mutant strain carrying *rodZ* expression plasmid pBAD-rodZ (Fig 2B). The difference between the wild-type and the *rodZ* mutants at 30 °C was greater for the *invE–lacZ* translational-fusion construct (Fig 2C). Consistently, the introduction of pBAD-rodZ into the *rodZ* mutant decreased β-galactosidase activity to the level of the wild-type strain. The results suggest that mutation of *rodZ* affects the expression of virulence genes at a post-transcriptional step.

Stability of *invE*-mRNA in the *rodZ* mutant

To confirm the prediction that RodZ has a function similar to that of the RNA chaperone Hfq, the stability of *invE*-mRNA in the *rodZ* mutant was measured after addition of rifampicin, a potent inhibitor of transcription initiation. In the wild-type strain MS390, *invE*-mRNA was degraded rapidly at 30 °C. By contrast, the basal level of *invE*-mRNA in the *rodZ* mutant was elevated, compared with the wild-type strain. Moreover, *invE*-mRNA remained stable for at least 30 min (Fig 3A). As determined by reverse transcription-PCR, the half-life of *invE*-mRNA was estimated to be more than 20 min in the *rodZ* mutant (Fig 3A), whereas in the *hfq* mutant this was approximately 5.8 min (Mitobe *et al*, 2008). Thus, the mutation of *rodZ* enhanced *invE*-mRNA stability more than the mutation of *hfq*. These results indicate a functional relationship between RodZ expression and *invE*-mRNA stability, which might suggest that the cytoskeletal protein RodZ has RNA-binding activity.

RodZ-*invE* RNA interaction *in vitro*

To determine whether RodZ interacts directly with *invE*-mRNA, a recombinant His-tagged *S. sonnei* RodZ fusion protein was purified to remove trace amounts of nuclease activity. Purified RodZ-His_6 formed a single band when analysed by 5–15% SDS–polyacrylamide gel electrophoresis (Fig 4A) and bound to an *invE* RNA probe in a gel-shift assay (Fig 4B). To assess the strength of the RodZ–*invE* RNA interaction, the apparent dissociation constant (K_d) was determined by measuring the disappearance of the RNA probe in a gel-shift assay. The apparent K_d for the formation of the RodZ–*invE* RNA complex was 3.5 nM (Fig 4C), which was significantly higher than that found for the Hfq–*invE* RNA ($K_d = 19.2$ nM for the monomer under similar experimental conditions; Mitobe *et al*, 2008). The interaction of RodZ–*invE* with RNA was not detected in buffer with 300 mM potassium glutamate (data not shown), which suggests that the affinity could be lower than the estimated values under physiological conditions.

To examine the specificity of RodZ binding to RNA, an *invE* DNA probe with the same sequence as the RNA probe was constructed and subjected to a gel-shift assay. The *invE* DNA probe did not form complexes with 2 nM RodZ (Fig 4D). Low concentrations of unlabelled *invE* RNA interfered with the formation of RodZ–*invE* RNA complexes (Fig 4B), and the inhibition of the RodZ–*invE* RNA interaction required high concentrations of calf thymus DNA, yeast transfer-RNA or polyphosphate (0.1–1 mg/ml; supplementary Fig S2 online). Binding of RodZ to RNA with an unrelated sequence, such as the 149-nucleotide *bla* RNA probe, was weak (Fig 4E). These data suggest that RodZ has high specificity for its substrate and nucleotide sequence.

RodZ–*invE* RNA interaction *in vivo*

To detect *in vivo* interactions between RNA and RodZ, MS5401 cells expressing His-tagged RodZ were exposed to ultraviolet light in the mid-logarithmic phase of growth, to crosslink RodZ to its target RNA. His-tagged RodZ–RNA complexes were purified from the cell lysate using magnetic beads. After washing with a high-salt buffer, the complexes were dissociated from the beads, and the crosslinked RodZ–RNA complexes were subjected to protease digestion. After subsequent treatment with RNase-free DNaseI, *invE* and *virF* mRNAs in the samples were detected by complementary-DNA synthesis and then by real-time PCR using specific photosequencing probes. The results shown in Fig 4F indicate that the level of *invE*-mRNA (red line) in the ultraviolet-treated sample was higher than that found in samples from cells without ultraviolet treatment (purple line) or from cells that did not express Hig-tagged RodZ (green line). Binding specificity was examined by measuring *virF* mRNA as an unrelated mRNA species within the same sample. The relative level of *virF* mRNA was 2^4- to 2^5-fold lower than that of *invE*-mRNA, as determined by the deviation of amplification plots against positive controls using an intact total RNA (blue line).

Signals were similarly detected in samples grown at 30 °C. The difference to that obtained at 37 °C was a rightward shift of total plots including the positive control, which is in agreement

©2011 EUROPEAN MOLECULAR BIOLOGY ORGANIZATION

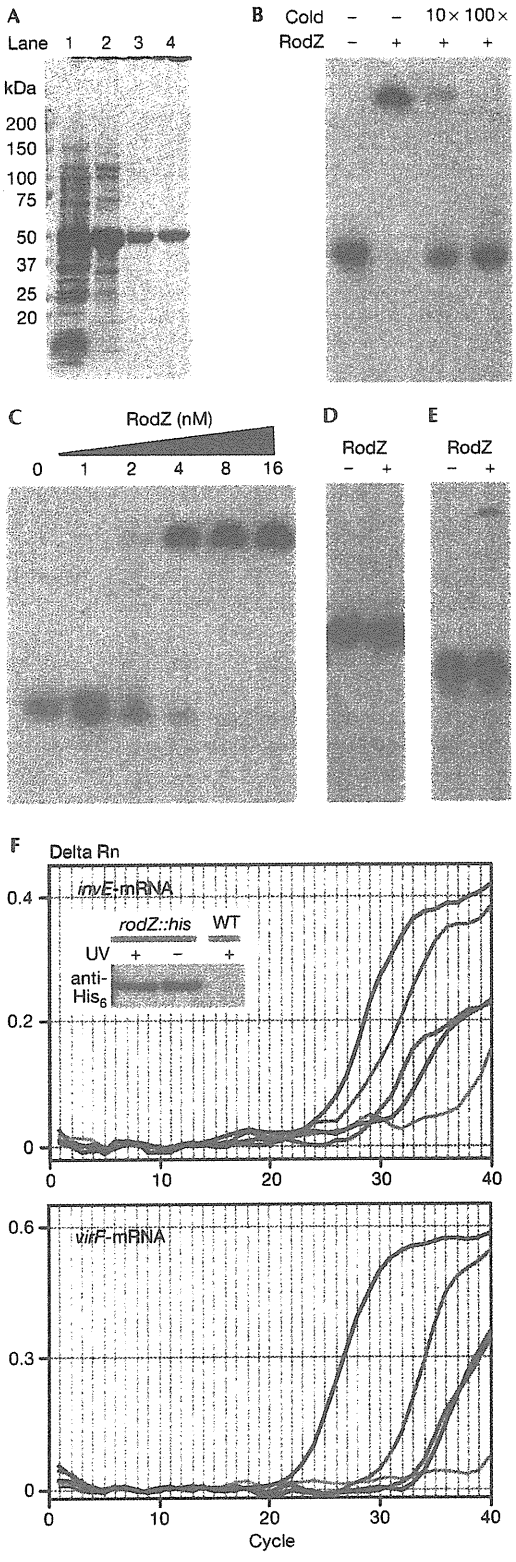

◀ **Fig 4** | RodZ–*invE* RNA binding. (A) Purified RodZ protein. Lane: 1, crude extract; 2, SP Sephadex; 3, P-11 phosphocellulose; 4, Ni-TED. (B) Gel-shift analysis of RNA binding using *invE* RNA probe (2 nM) and RodZ (16 nM). Cold: 10- and 100-fold unlabelled *invE* RNA. (C) Determination of the apparent K_d of the RodZ–*invE* RNA-binding interaction. A constant amount of RNA (2 nM) was mixed with the indicated amounts of RodZ. (D) Gel-shift analysis of the RodZ–*invE* DNA interaction using 2 nM *invE* PCR product and RodZ (16 nM). (E) Gel-shift analysis of the RodZ–*bla*-RNA interaction using 2 nM RNA probe and RodZ (16 nM). (F) Detection of *in vivo invE* and *virF* mRNA binding at 37 °C by real-time PCR. Blue, positive control by 10 ng total RNA; red, *invE*-mRNA–RodZ::His_6 complex from crosslinked MS5401 (*rodZ::his*$_6$) strain; purple, negative control from uncrosslinked MS5401 strain; green, negative control from crosslinked wild-type strain; cyan, RNaseA-treated sample from crosslinked MS5401 strain. Tethered RNA–protein complex for the complementary DNA synthesis was detected by His_6 antibody. mRNA, messenger RNA; UV+, ultraviolet-irradiated samples; UV−, no treatment; WT, wild type.

with the fact that little difference was observed in RNA-binding activity *in vitro* at either temperature (data not shown). This suggests that the temperature dependency of the *invE*-mRNA degradation might depend on an as yet unidentified factors such as Hfq, which shows temperature-dependent RNA-binding activity *in vitro* (Mitobe *et al*, 2008).

Functional mapping of RodZ

These results indicated that RodZ has RNA-binding activity with significant specificity in addition to its role as a cytoskeletal protein in rod-shaped bacteria. RodZ contains a helix-turn-helix (HTH) motif in the N-terminal region and a short basic region (KRRKKR) near the transmembrane domain (Shiomi *et al*, 2008; Bendezu *et al*, 2009). To identify the region necessary for RNA binding, a protein variant with an internal deletion of the short basic region (ΔKRRKKR) was constructed. This mutation resulted in the loss of RodZ RNA-binding activity *in vitro*, which shows that this region is essential for RNA binding (supplementary Fig S3B online). However, when a plasmid expressing ΔKRRKKR RodZ was introduced into a *rodZ* mutant, InvE expression was repressed as much as in the transformant with the wild-type *rodZ* expression plasmid (Fig 5A, lanes 2 and 4). Therefore, the deletion of only KRRKKR was not sufficient to interfere with RodZ–*invE*-mRNA processing *in vivo*.

RodZ also has several conserved, basic amino-acid residues in a short segment between the HTH domain and KRRKKR (NCBI Conserved Domain no. PRK10856). By using the *rodZ* ΔKRRKKR mutant, each of these three Arg residues (R62, R70 and R90) was substituted with Gly (supplementary Fig S3A online). The *rodZ* mutants carrying expression plasmids with one or two Arg substitutions repressed expression of InvE in a manner that was similar to the *rodZ* mutant carrying the wild-type *rodZ* expression plasmid (Fig 5A, lane 5–10). However, the expression of a *rodZ* mutant with all three Arg substitutions (R62G, R70G and R90G) did not repress InvE expression (Fig 5A, lane 11). This increase in production of InvE protein was accompanied by increased stability of *invE*-mRNA (supplementary Fig S3C online). In addition, a plasmid encoding an R62G, R70G and R90G *rodZ* allele without deletion of KRRKKR repressed InvE synthesis (Fig 5A, lane 12). Taken together, these results suggest that the short basic region (KRRKKR) and the three additional Arg residues have important roles in the repression of InvE synthesis *in vivo*.

©2011 EUROPEAN MOLECULAR BIOLOGY ORGANIZATION

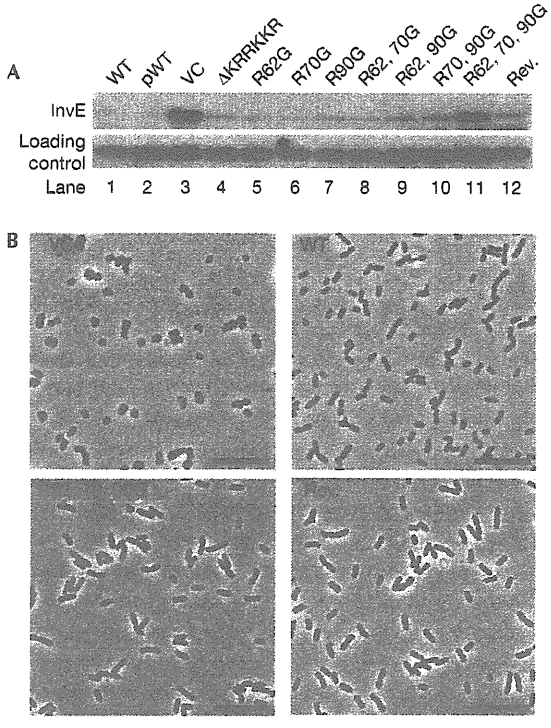

Fig 5 | Functional domain mapping. (A) Immunoblot analysis of InvE protein at 30 °C in MS5201 (Δ*rodZ*) strains carrying the indicated expression plasmids. Lanes: 1, WT MS390; 2, Δ*rodZ* strain carrying pBAD-rodZ; 3, VC; 4, ΔKRRKKR; 5, R62G; 6, R70G; 7, R90G; 8, R62G, R70G; 9, R62G, R90G; 10, R70G, R90G; 11, R62G, R70G, R90G; 12, R62G, R70G, R90G with KRRKKR (Rev.). (B) Phase contrast images of strain MS5201 (Δ*rodZ*) expressing the indicated RodZ variants. Scale bars, 10 μm. Rev., reversion of the short basic region; VC, vector control; WT, wild type.

Finally, the influence of *rodZ* mutations on cell shape was investigated. The *rodZ* mutant with a plasmid encoding all three Arg substitutions, with or without the short basic region (KRRKKR), adopted the same cell shape as a *rodZ* mutant that harboured the wild-type *rodZ* plasmid (Fig 5B). This shows that neither the substitution of the three Arg residues nor the deletion of the short KRRKKR basic region of RodZ influences the cell shape. Thus, the RodZ protein might have two functions: an architectural role in the cytoskeleton and a regulatory role for processing mRNA.

Our experimental results indicate that RodZ and *invE*-mRNA interact directly in living cells, leading to post-transcriptional repression of InvE synthesis due to the decreased stability of *invE*-mRNA. However, repression of InvE synthesis was observed in the *rodZ* mutant expressing ΔKRRKKR RodZ (Fig 5A, lane 4) even though this mutant RodZ had lost its RNA binding *in vitro* (supplementary Fig S3B online). One explanation for this apparent contradiction is that for effective interaction of RodZ with *invE*-mRNA, an auxiliary factor is involved that restores the *invE*-repression activity in mutants lacking one of the two elements, the KRRKKR sequence or the three Arg residues (Fig 5A, lanes 4 and 12). However, this putative cofactor was unable to restore the activity of the mutant lacking both elements (Fig 5A, lane 11). Taken together, we speculate that either of the elements is sufficient for completion of post-transcriptional repression. RodZ might mediate spatial coincidence between the processed mRNA and putative factors for post-transcriptional regulation. Further analysis of RodZ immunoprecipitates—in which we have already observed more than 12 unidentified bands following SDS–polyacrylamide gel electrophoresis—should resolve this issue.

The precise role of the three Arg residues, which were initially suggested to be additional RNA-binding sites, remains to be elucidated. Crystal structure of the cytoplasmic domain of RodZ in *Thermotoga maritime* shows that the Arg residues are predicted to exist in the fourth and fifth helices. Proper conformation of the fourth helix is important because amino-acid substitutions F60A and Y64A in a GFP-RodZ$^{1-138}$-RFP are unable to interact with MreB, and result in round cells (van den Ent *et al*, 2010). Dissimilarly to aromatic amino-acids, substitution of the three Arg residues might not cause drastic changes in the conformation of the helix motif, as the shape of bacteria expressing those variants did not change (Fig 5B). RodZ has an additional Arg residue at the 66th amino acid. Addition of the further R66G substitution to the three Arg substitutions with ΔKRRKKR, however, resulted in a round cell-shape, but not by a single R66G substitution (data not shown). These results suggest that a subtle change of protein structure, which could disrupt putative interaction with the cofactor or additional RNA-binding sites, had already occurred in the mutant of three Arg substitutions with ΔKRRKKR.

Our results support a hypothesis that there are two fundamental roles for RodZ in rod-shaped bacteria: to maintain proper cytoskeletal architecture and to function in mRNA processing. As RodZ is localized to the membrane, it might function as an anchor to position nascent mRNA molecules. The recent discovery of an RNaseE complex that also localizes to the membrane (Taghbalout & Rothfield, 2008) supports the idea that post-transcriptional regulation occurs in spaces adjacent to the membrane. Thus, membrane-bound RodZ might provide a platform for post-transcriptional regulation.

METHODS

Bacterial strains and plasmids. Bacterial strains and plasmids used in this study are listed in supplementary Table SI online.

Genetic screening. The EZ-Tn*5*<KAN-2> transposome (Epicenture) was introduced by electroporation into *E. coli* strain ME2824, which carries the *mxiC*(TTSS)–*lacZ* fusion plasmid, pJM1718. Transformants were plated on LB X-gal agar with kanamycin and chloramphenicol and incubated overnight at 37 °C.

Purification of RodZ and gel-shift assays. Recombinant RodZ-His$_6$ protein was expressed in *E. coli* BL21(DE3) (Novagen) carrying pET22b-RodZ plasmid, purified by Hi-prep SP (GE Healthcare) and P-11 phosphocellulose (Whatman), followed by Ni-TED column (Macherey Nagel). For gel-shift assay, RodZ was mixed with 20 femtomoles of labelled RNA probe consisting of the first 140 nucleotides of the *invE* gene in a 10 μl of RNA-binding buffer, as described previously (Mitobe *et al*, 2008).

***In vivo* crosslinking of mRNA.** A volume of 12 ml of MS5401 culture (OD_{600} = 1.0 at 37 °C) was subjected to ultraviolet crosslinking under a fluence of 0.2 J/cm^2 ultraviolet-B (45 s, Funa UV linker FS800, Funakoshi) at 4 °C. The cells were lysed in 1 ml of binding buffer and mixed with 12.5 μl of Dynabeads TARON (Dynal), which was pretreated with a lysate of avirulent MS506 strain. After 30 min binding at 4 °C, the beads were collected

©2011 EUROPEAN MOLECULAR BIOLOGY ORGANIZATION

and extensively washed by saturated ammonium sulphate (pH 8.0). RNA–protein complexes were released from beads, and treated by Turbo DNase kit (Ambion). The sample was subjected to complementary DNA synthesis and real-time PCR by ABI PRISM 7000 using photoquencing probes against *invE* and *virF* genes.

Supplementary information is available at EMBO *reports* online (http://www.emboreports.org).

ACKNOWLEDGEMENTS

We thank Y. Horiuchi from the Life Science Research Institute, Kinki University, for assistance with electron microscopy; M. Ino from Saitama Prefectural University for her kind assistance with biochemical analyses; and Dr M. Wachi from the Tokyo Institute of Technology for providing the A22 reagent. This research was supported by a grant-in-aid from the Ministry of Health, Labor and Welfare of the Japanese Government (H21 · kokusai-igaku).

CONFLICT OF INTEREST

The authors declare that they have no conflict of interest.

REFERENCES

Adler B, Sasakawa C, Tobe T, Makino S, Komatsu K, Yoshikawa M (1989) A dual transcriptional activation system for the 230 kb plasmid genes coding for virulence-associated antigens of *Shigella flexneri*. *Mol Microbiol* **3:** 627–635

Alves R, Savageau MA (2003) Comparative analysis of prototype two-component systems with either bifunctional or monofunctional sensors: differences in molecular structure and physiological function. *Mol Microbiol* **48:** 25–51

Alyahya SA, Alexander R, Costa T, Henriques AO, Emonet T, Jacobs-Wagner C (2009) RodZ, a component of the bacterial core morphogenic apparatus. *Proc Natl Acad Sci USA* **106:** 1239–1244

Beloin C, Dorman CJ (2003) An extended role for the nucleoid structuring protein H-NS in the virulence gene regulatory cascade of *Shigella flexneri*. *Mol Microbiol* **47:** 825–838

Bendezu FO, Hale CA, Bernhardt TG, de Boer PA (2009) RodZ (YfgA) is required for proper assembly of the MreB actin cytoskeleton and cell shape in *E. coli*. *EMBO J* **28:** 193–204

Dorman CJ, Porter ME (1998) The *Shigella* virulence gene regulatory cascade: a paradigm of bacterial gene control mechanisms. *Mol Microbiol* **29:** 677–684

Jones LJ, Carballido-Lopez R, Errington J (2001) Control of cell shape in bacteria: helical, actin-like filaments in *Bacillus subtilis*. *Cell* **104:** 913–922

Kato J, Ito K, Nakamura A, Watanabe H (1989) Cloning of regions required for contact hemolysis and entry into LLC-MK2 cells from *Shigella sonnei* form I plasmid: *virF* is a positive regulator gene for these phenotypes. *Infect Immun* **57:** 1391–1398

Maurelli AT, Blackmon B, Curtiss R III (1984) Temperature-dependent expression of virulence genes in *Shigella* species. *Infect Immun* **43:** 195–201

Mitobe J, Arakawa E, Watanabe H (2005) A sensor of the two-component system CpxA affects expression of the type III secretion system through posttranscriptional processing of InvE. *J Bacteriol* **187:** 107–113

Mitobe J, Morita-Ishihara T, Ishihama A, Watanabe H (2008) Involvement of RNA-binding protein Hfq in the post-transcriptional regulation of *invE* gene expression in *Shigella sonnei*. *J Biol Chem* **283:** 5738–5747

Mitobe J, Morita-Ishihara T, Ishihama A, Watanabe H (2009) Involvement of RNA-binding protein Hfq in the osmotic-response regulation of *invE* gene expression in *Shigella sonnei*. *BMC Microbiol* **9:** 110

Nakayama S, Watanabe H (1998) Identification of *cpxR* as a positive regulator essential for expression of the *Shigella sonnei virF* gene. *J Bacteriol* **180:** 3522–3528

Porter ME, Dorman CJ (1994) A role for H-NS in the thermo-osmotic regulation of virulence gene expression in *Shigella flexneri*. *J Bacteriol* **176:** 4187–4191

Shiomi D, Sakai M, Niki H (2008) Determination of bacterial rod shape by a novel cytoskeletal membrane protein. *EMBO J* **27:** 3081–3091

Taghbalout A, Rothfield L (2008) New insights into the cellular organization of the RNA processing and degradation machinery of *Escherichia coli*. *Mol Microbiol* **70:** 780–782

van den Ent F, Johnson CM, Persons L, de Boer P, Lowe J (2010) Bacterial actin MreB assembles in complex with cell shape protein RodZ. *EMBO J* **29:** 1081–1090

Watanabe H, Arakawa E, Ito K, Kato J, Nakamura A (1990) Genetic analysis of an invasion region by use of a Tn*3-lac* transposon and identification of a second positive regulator gene, *invE*, for cell invasion of *Shigella sonnei*: significant homology of *invE* with ParB of plasmid P1. *J Bacteriol* **172:** 619–629

©2011 EUROPEAN MOLECULAR BIOLOGY ORGANIZATION

ELSEVIER

Brain & Development 34 (2012) 20–27

BRAIN & DEVELOPMENT
Official Journal of the Japanese Society of Child Neurology

www.elsevier.com/locate/braindev

Original article

Thermolabile CPT II variants and low blood ATP levels are closely related to severity of acute encephalopathy in Japanese children

Masaya Kubota [a,b], Junji Chida [c], Hideki Hoshino [a], Hiroshi Ozawa [b], Ayaka Koide [b], Hirohumi Kashii [a,b], Akiko Koyama [a], Yoko Mizuno [b], Ai Hoshino [b], Miyoko Yamaguchi [c], Dengbing Yao [c], Min Yao [c], Hiroshi Kido [c,*]

[a] *Division of Neurology, National Center for Child Health and Development, 2-10-1 Ohkura, Setagaya-Ku, Tokyo, Japan*
[b] *Department of Pediatrics, Metropolitan Hachioji Children's Hospital, Tokyo, Japan*
[c] *Division of Enzyme Chemistry, Institute for Enzyme Research, The University of Tokushima, Kuramoto-cho 3-18-15, Tokushima 770-8503, Japan*

Received 5 May 2010; received in revised form 10 October 2010; accepted 27 December 2010

Abstract

Despite the decrease in Reye syndrome after the discontinuation of aspirin, acute encephalopathy (non-Reye syndrome type) has been continually reported in Japan. Recent studies suggested that the thermolabile phenotype of carnitine palmitoyltransferase II (CPT II) variation [F352C] was closely related to the pathomechanism of influenza-associated encephalopathy (IAE) in Japanese, causing mitochondrial ATP utilization failure during periods of high fever, resulting in brain edema. So, we analyzed CPT II polymorphism and peripheral blood ATP levels as a signal of "energy crisis" in 12 and 10 patients with acute encephalopathy, respectively. Out of the 12 patients with acute encephalopathy, six showed thermolabile CPT II variants [F352C], and of these six, two patients died in spite of intensive care. In contrast, the remaining six patients with no thermolabile CPT II variant [F352C] showed a relatively mild clinical course. Blood ATP levels of the 10 patients in the acute phase of encephalopathy were significantly lower than those during the convalescent phase and also those of patients with febrile seizure status. Our data suggest that the thermolabile F352C CPT II variant, found only in Japanese, might be one of the predisposing factors to trigger the pathomechanism of acute encephalopathy in the Japanese population, and that it is causally related to the severity of disease. The decreased blood ATP level seems to reflect systemic mitochondrial dysfunction including the blood brain barrier during the acute phase of encephalopathy.
© 2011 The Japanese Society of Child Neurology. Published by Elsevier B.V. All rights reserved.

Keywords: Acute encephalopathy, Carnitine palmitoyltransferase II; Thermolabile variants; ATP; Mitochondrial dysfunction

1. Introduction

Acute encephalopathy in children is clinically characterized by high fever, prolonged consciousness disturbance associated with brain edema, and prolonged or multiple generalized seizures. Acute encephalopathy distinct from Reye syndrome is not rare in Japan. The precise pathogenesis of acute encephalopathy including influenza-associated encephalopathy (IAE) remains unclear. An epidemiological study revealed that aspirin use was closely related to the pathogenesis of Reye syndrome [1]. However, despite the decrease in Reye syndrome after the discontinuation of aspirin, acute encephalopathy (non-Reye syndrome type) has been continually reported in Japan [2].

Recently, acute encephalopathy was classified into several types according to magnetic resonance imaging (MRI) findings together with the clinical course, such

* Corresponding author. Tel.: +81 88 633 9649; fax: +81 88 633 7425.
E-mail address: kido@ier.tokushima-u.ac.jp (H. Kido).

0387-7604/$ - see front matter © 2011 The Japanese Society of Child Neurology. Published by Elsevier B.V. All rights reserved.
doi:10.1016/j.braindev.2010.12.012

as acute necrotizing encephalopathy [3], acute encephalopathy with biphasic seizures and late reduced diffusion [4], and hemorrhagic and shock encephalopathy [5,6]. Although the influenza virus and HHV-6 (human herpes virus-6) are the main causative agents of these acute encephalopathies, many other viruses are also considered to be responsible for the disease [3,4,7].

It is estimated that more than 100 children die of IAE every year in Japan [8,9]. According to the first nationwide clinical survey of IAE in Japan, in many patients with IAE, multiple-organ failure developed, and rates of mortality (31.8%) and disability (27.7%) were high [2]. Although clinical and neuropathological studies suggested that blood–brain barrier destruction and hypercytokinemia in cerebrospinal fluid were closely related to the pathogenesis of IAE, the pathophysiology and mechanisms of disease onset are still unclear [3,7,10,11].

Recently, Chen et al. [12] reported that the thermolabile phenotypes of carnitine palmitoyltransferase II (CPT II) variations, [1055T > G/F352C] alone, and [1055T > G/F352C] + [1102G > A/V368I] were closely related to the pathomechanisms of IAE. The CPT system is a pivotal component of ATP generation through mitochondrial fatty acid oxidation in mammals [13]. Yao et al. [14] further characterized the enzyme properties of the CPT II variants as follows: (1) dominant-negative effect, (2) reduced activities, (3) thermal instability, and (4) short half-lives compared with the wild-type. They demonstrated that the thermolabile CPT II variants might cause mitochondrial fuel utilization failure in various organs and endothelial cells during periods of high fever, and, thus, might play an important role in the pathogenesis of brain edema in IAE. In the present study, we analyzed the CPT II polymorphism and peripheral blood ATP levels as a signal of "energy crisis" in patients with acute encephalopathy with and without influenza virus infection, septic encephalopathy, and febrile delirium during influenza virus infection, and analyzed the relationships among these data, age, and clinical manifestations.

2. Patients and methods

2.1. Patient profile for the study of CPT II polymorphism

This investigation was approved by the Ethics Review Committee for human genome analysis of our institution. All participants' caregivers gave written informed consent. Fifteen patients were included in the study. The clinical details are summarized in Table 1. The diagnoses of the 15 patients were as follows: 12 patients with acute encephalopathy (7 IAE, one human herpes virus type 6 (HHV-6) associated, one varicella-associated, one septic encephalopathy associated with *Hemophilus influenzae* type b, two acute encephalopathy with an unknown pathogenesis, highly suspected of being of viral origin), and three febrile delirium associated with influenza virus infection. Two patients (Case 1, IAE, and Case 2, septic encephalopathy) died 30 and 3 days after admission, respectively, despite intensive care. All 12 patients with acute encephalopathy were diagnosed based on prolonged seizures with high fever and/or consciousness disturbance lasting longer than 12 h associated with brain CT or MRI abnormalities.

3. Representative case presentations

3.1. Case 1

This 4-year-old girl was admitted to our hospital because of feeding difficulty, a lethargic state, and high fever lasting longer than 12 h. A rapid test for influenza A virus antigen in the nasal discharge was positive. She has been followed at our outpatient clinic with a diagnosis of severe psychomotor delay and epilepsy due to chromosome abnormality (46, XX, dup(2)(q21.1q24.2)) since the age of 3 years. Her seizure disorder was well-controlled with phenobarbital. On admission, except for a lethargic tendency, she showed no neck stiffness, involuntary movement, or convulsion, and her respiratory and circulatory conditions were stable. She was also able to follow an object. Neurological examination revealed normal light and corneal reflexes and normal deep tendon reflexes. Pathological reflexes were not induced. Her consciousness level, however, deteriorated 12 h after admission. On laboratory tests, blood glucose, ammonia, the white blood cell count (WBC), hemoglobin (Hb), and platelet count (Plt) were within normal ranges, and cereblospinal fluid (CSF) findings were unremarkable. Blood and CSF cultures were negative. Because she also showed sudden respiratory insufficiency and reduced blood pressure, she was immediately resuscitated and intubated. After that, she could not move and all brainstem reflexes disappeared. On brain CT the next day, as shown in Fig. 1a, cisterns surrounding the brainstem and cerebellum were not identified and auditory brainstem responses (ABR) showed only bilateral wave I. Rapid consciousness deterioration as well as brain CT and ABR findings suggested cerebral herniation due to influenza-associated brainstem encephalopathy. On the second CT 3 weeks later, severe brain edema and subarachnoid hemorrhage were observed. Despite intensive care, she died on the 31st day of hospitalization. She had a thermolabile F352C CPT II variant.

3.2. Case 2

This previously healthy 2-year-old boy was admitted to our hospital because of consciousness disturbance, a brief seizure cluster, and high fever lasting 24 h. On admission, neurological examination revealed coma, the absence of light and corneal reflexes, dilated and anisocoric pupils, and flaccid extremities. Neck stiffness was

Table 1
Clinical summary of patients and CPT II polymorphism.

Case no.	Age at onset	Pathogen	Diagnosis	CPT II polymorphism	Duration of high fever	Duration of seizure (min)	Therapy	Outcome
1[c]	4 years 10 months	Flu A	IAE	F352C	24 h	(−)	Gly, IVIG, m-PSL, Venti	Died
2	2 years 2 months	*H. influenza*	Hib septic AE	F352C, V368I	2 days	3	Venti, Epin, DOA, CTX	Died
3[c]	1 year	Unknown	AEU	F352C, V368I	2 days	30	Mann, MDZ	Severe MR, MD, Epi
4[c]	1 year 7 months	Flu A	IAE	(−)	30 h	40	Gly, m-PSL, Venti	Moderate MR, MD, Epi
5[a]	4 years 5 months	Flu A	IAE	F352C, V368I	5 days	90	Gly, MDZ, Pen, IVIG, m-PSL	Moderate MR
6[a]	2 years 1 months	Varicella	Varicella AE	F352C, V368I	24 h	90	Mann, MDZ, m-PSL	Mild MR
7[c]	6 years	Unknown	AEU	F352C, V368I	2 days	30	Mann, MDZ, m-PSL, HT	Mild MR
8[a]	1 years 4 months	Flu A	IAE	V368I	5 days	60	Gly, MDZ, Pen, PB, m-PSL	Mild MR
9[a]	2 years	Flu A	IAE	V368I	5 days	60	Gly, MDZ, Pen, IVIG, m-PSL	Mild MR
10[a]	11 months	HHV-6	HHV-6 AE	V368I	36 h	100	Gly, MDZ, Pen, m-PSL	Good
11[b]	2 years 5 months	Flu A	IAE	V368I, M647 V	24 h	40	MDZ, PB, m-PSL, HT	Good
12[a]	3 years 11 months	Flu A	IAE	V368I	2 days	40	MDZ, PB, m-PSL, HT, Venti	Good
13	4 years 9 months	Flu A	FD	F352C, V368I	4 days	2	(−)	Good
14	9 years 5 months	Flu A	FD	(−)	3 days	(−)	(−)	Good
15	11 years	Flu A	FD	V368I, M647V	3 days	(−)	(−)	Good

IAE: Influenza-associated encephalopathy, AEU: acute encephalopathy of unknown pathogen, FD: febrile delirium, Flu A: influenza A, HHV-6: human herpes virus-6, MR; mental retardation, MD: motor delay, Epi: epilepsy, Mann: mannitol, MDZ: midazolam, m-PSL: methylpredonisolone, HT: hypothermia, Venti: artificial ventilator, Epin: epinephrine, DOA: dopamine, CTX: cefotaxim, PB: Phenobarbital, Pen: pentobarbital, IVIG: intravenous infusion of gamma-globlin, Gly: glycerole.

[a] AESD (acute encephalopathy with biphasic seizures and late reduced diffusion).

[b] This case partially resembles ANE (acute necrotizing encephalopathy).

[c] Unclassified acute encephalopathy.

not observed. A rapid test for influenza virus antigen in the nasal discharge was negative. His head CT demonstrated diffuse brain edema, as shown in Fig. 1b. On laboratory investigation, blood glucose and ammonia, as well as liver and renal functions were within normal limits. WBC was 18,000/μL, Hb 11.6 g/dL, Plt 3,60,000/μL, and prothrombin time 68.7 s. Blood culture identified *H. influenzae* type b. Spinal tap was not performed because of the risk of cerebral herniation. The blood ATP level was 0.58 mM on admission. The acylcarnitine ratio ((C16 + C18:1)/C2) was high, at 0.203, on admission, compared with the upper cutoff value of 0.048 [12]. We diagnosed him with septic encephalopathy. Despite intensive care including antibiotics, ventilator support, and catecholamine infusion, he died 2 days later. He had compound thermolabile CPT II variants [F352C + V368I].

3.3. Case 12

This previously healthy 3-year-old boy was admitted to our hospital because of a febrile seizure status and high fever lasting longer than 24 h. His generalized tonic clonic seizure was suppressed with pentobarbital infusion 40 min after the onset. A rapid test for influenza virus antigen in the nasal discharge was positive for flu A. Brain CT revealed mild brain edema. So, he was sedated and intubated. Methylpredonisolone (m-PSL) pulse and hypothermia therapies were immediately started based on the diagnosis of IAE. The blood ATP value was 0.77 mM on admission, and it increased to 1.35 mM 2 weeks later. On the 6th day of hospitalization, he developed brief right-sided clonic seizure. Brain MRI (diffusion-weighted images) showed an abnormal high intensity in the left hemisphere (Fig. 1e). The clinical course and MRI findings were compatible with acute encephalopathy with biphasic seizures and late reduced diffusion [4]. Additional m-PSL therapy was given and the hypothermia therapy gradually discontinued. His neurological condition subsequently showed a full recovery. No apparent mental, motor, and social skill impairment was noted during follow-up 1 year later. He had a V368I CPT II variant.

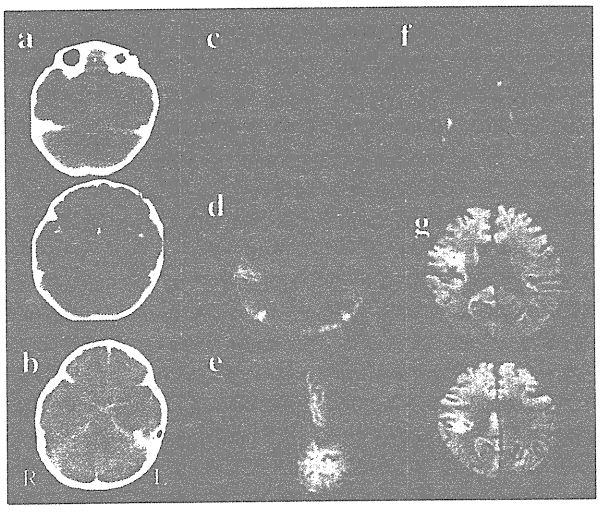

Fig. 1. (a) Brain CTs on 2nd and 21st day of hospitalization in Case 1 showing disappearance of cistern between brainstem and cerebellum (upper image) and severe brain edema (lower image). (b) Brain CT on admission showing severe brain edema in Case 2. (c–g) Brain MRIs showing abnormal high intensities in diffusion-weighted images in Cases 6,7,12,11 and 10, respectively.

3.4. Patient profile for the study of the blood ATP level

Twenty-five patients were included in this study. The diagnoses of the 25 patients were as follows: 10 patients with acute encephalopathy (mean age: 3 years and 11 months, age range: 7 months–10 years and 8 months, one IAE, one *Salmonella*-associated, one HHV-6-associated, three unknown virus-associated, one methylmalonic aciduria, one hepatic encephalopathy, one hemolytic uremic syndrome, and one septic encephalopathy (Case 2 in Table 1)), nine febrile seizure status (mean age: 1 year and 5 months, age range: 4 months–4 years 9 months), and six mitochondrial disease (mean age: 9 years and 8 months, age range: 2–25 years, two partial cytochrome c oxidase deficiency, three Leigh syndrome, and one chronic progressive external ophthalmoplegia). All 10 patients with acute encephalopathy were analyzed regarding the blood ATP levels in the acute phase (within 24 h of disease onset), and five of the 10 patients were also analyzed in the convalescent phase. Among the 15 patients who were analyzed for CPT II polymorphism, only Cases 2 and 12 were included in this study.

4. Methods

4.1 Analysis of CPT II polymorphism

Genomic DNA from whole blood was purified as previously described [15]. PCR of five exons of the CPT II gene was carried out with intron-based primers in genomic DNA. For haplotype analysis, the CPT II exon four region was cloned into the pCR® 2.1 vector (Invitrogen). The sequences of the PCR products and cloned CPT II gene were analyzed employing the ABI DyeDeoxy Terminator Cycle Sequencing Kit with an ABI-PRISM 3100 Genetic Analyzer (PE-Applied Biosystems). Each PCR product was sequenced at least twice independently.

4.2. Preparation of patients' lymphoblasts and culture

Blood samples (2 mL) were obtained from patients by venipuncture into a sterile EDTA blood collection tube. Lymphocytes were separated from peripheral blood, diluted (1:1, v/v) with sterile saline, by centrifugation (800×*g*, 20 min) over 2 mL of Lymphoprep (Nycomed). The lymphocyte layer was recovered and washed twice with PBS by centrifugation at 250×*g* for 10 min each, and then maintained in PRMI-1640 (GIBCO) supplemented with 12.5% FCS. Cells were incubated with 5% CO_2 at 37 °C for 7 days. Lymphoblastic cell lines were established by infecting peripheral blood lymphocytes with the Epstein Barr virus. Cells were grown in suspension in an SC flask (Greiner 658190) in an upright position, in 10 ml of PRMI-1640 medium that contained 12.5% FCS, maintained at 37 °C. Fluid was routinely changed every 2 days by removing the medium above the settled cells and replacing it with an equal volume of fresh medium.

4.3. Analysis of CPT II activity

CPT II activities of patients' lymphoblasts were analyzed as previously described [14]. To prepare whole cell extracts, cells were harvested and washed twice with PBS (−) at 250×*g* for 10 min and then lysed with 0.5 mL of ice-cold lysis buffer (5 mM Tris–HCl buffer, pH 7.4, containing 1% Tween-20 and 0.5 M KCl), then centrifuged at 147,600×*g* for 1 h at 4 °C. To analyze the heat stability of CPT II, cell lysates were pre-incubated at 30, 37 and 41 °C for 0–120 min. Protein concentrations in the cell lysates were measured using the BCATM Protein Assay Kit (Thermo SCIENTIFIC).

4.4. Measurement of blood ATP levels

ATP concentrations in whole blood lysate were measured by an ENLITEN® ATP assay system bioluminescence detection kit (Promega) according to the instructions provided by the manufacturer and the values were expressed as ATP levels in whole blood.

5. Results

5.1. CPT II polymorphism in the patients

As shown in Table 1, among the 15 patients studied, seven had a thermolabile F352C CPT II variant (1 F352C only and six [F352C + V368I]), four V368I only,